The value of hyperspectral UAV imagery in characterizing tundra vegetation

Putkiranta, Pauli

Elsevier Inc.
2024-05-15

Putkiranta, P, Räsänen, A, Korpelainen, P, Erlandsson, R, Kolari, T H M, Pang, Y, Villoslada, M, Wolff, F, Kumpula, T & Virtanen, T 2024, 'The value of hyperspectral UAV imagery in characterizing tundra vegetation', Remote Sensing of Environment, vol. 308. https://doi.org/10.1016/j.rse.

http://hdl.handle.net/10138/593466
10.1016/j.rse.2024.114175

Remote Sensing of Environment 308 (2024) 114175

Contents lists available at ScienceDirect

Remote Sensing of Environment

journal homepage: www.elsevier.com/locate/rse

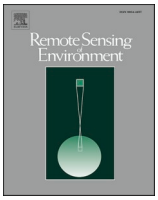

The value of hyperspectral UAV imagery in characterizing tundra vegetation

Pauli Putkiranta [a,*], Aleksi Räsänen [b,c], Pasi Korpelainen [d], Rasmus Erlandsson [e,f], Tiina H.M. Kolari [g,h], Yuwen Pang [a], Miguel Villoslada [d,i], Franziska Wolff [d], Timo Kumpula [d], Tarmo Virtanen [a]

[a] Ecosystems and Environment Research Programme, Faculty of Biological and Environmental Sciences, University of Helsinki, P.O. Box 65, Helsinki 00014, Finland
[b] Bioeconomy and Environment, Natural Resources Institute Finland, Paavo Havaksen tie 3, Oulu 90570, Finland
[c] Geography Research Unit, Faculty of Science, University of Oulu, P.O. Box 8000, Oulu 90014, Finland
[d] Department of Geographical and Historical Studies, University of Eastern Finland, P.O. Box 111, Joensuu 80101, Finland
[e] Department of Ecology, Environment and Plant Sciences, Stockholm University, Svante Arrhenius väg 20 A, Stockholm 106 91, Sweden
[f] Norwegian Institute for Nature Research (NINA), FRAM – High North Research Centre for Climate and the Environment, Tromsø, Norway
[g] Centre de recherche sur la dynamique du système Terre (GEOTOP), Université du Québec à Montréal, 201 Président-Kennedy Avenue, Montréal, QC H2X 3Y7, Canada
[h] Department of Environmental and Biological Sciences, University of Eastern Finland, Yliopistokatu 7, P.O. Box 111, Joensuu 80101, Finland
[i] Institute of Agriculture and Environmental Sciences, Estonian University of Life Sciences, Kreutzwaldi 5, Tartu 51014, Estonia

ARTICLE INFO

Editor: Jing M. Chen

Keywords:
Tundra
Plant communities
Multispectral imaging
Hyperspectral imaging
Drone
Biodiversity

ABSTRACT

The fine-scale spatial heterogeneity of low-growth Arctic tundra landscapes necessitates the use of high-spatial-resolution remote sensing data for accurate detection of vegetation patterns. While multispectral satellite and aerial imaging, including the use of uncrewed aerial vehicles (UAVs), are common approaches, hyperspectral UAV imaging has not been thoroughly explored in these ecosystems. Here, we assess the added value of hyperspectral UAV imaging relative to multispectral UAV imaging in modelling plant communities in low-growth oroarctic tundra heaths in Saariselkä, northern Finland. We compare three different spectral compositions: 4-channel broadband aerial images, 5-channel broadband UAV images and 112-channel narrowband UAV images. Based on field vegetation plot data, we estimate vascular plant aboveground biomass, leaf area index, species richness, Shannon's diversity index, and community composition. We use spectral and topographic information to compile 12 explanatory datasets for random forest regression and classification.

For aboveground biomass and leaf area index, the highest R^2 values were 0.60 and 0.65, respectively, and broadband variables were most important. In the best models for biodiversity metrics species richness and Shannon's index R^2 values were 0.53 and 0.46, respectively, with hyperspectral, topographic, and multispectral variables having high importance. For 4 floristically determined community clusters, both random forest classifications and fuzzy cluster membership regressions were conducted. Overall accuracy (OA) for classification was 0.67 at best, while cluster membership was estimated with an R^2 of 0.29–0.53. Variable importance was heavily dependent on community composition, but topographic, multispectral, and hyperspectral data were all selected for these community composition models. Hyperspectral models generally outperformed multispectral ones when topographic data were excluded. With topographic data, this difference was diminished, and performance improvements from added hyperspectral data were limited to 0–10 percentage point increases in R^2, the largest occurring in the metrics with lowest R^2. These results suggest that while hyperspectral can outperform multispectral imaging, multispectral and topographic data are mostly sufficient in practical applications in tundra heaths.

* Corresponding author.
E-mail address: pauli.putkiranta@helsinki.fi (P. Putkiranta).

https://doi.org/10.1016/j.rse.2024.114175
Received 27 November 2023; Received in revised form 19 April 2024; Accepted 28 April 2024
Available online 15 May 2024

1. Introduction

Remote sensing tools are vital in monitoring the impacts of climate and environmental change. In Arctic ecosystems, where amplification rates of global warming are up to four times the global average (Rantanen et al., 2022), large-scale climate change impacts include general greening, but closer analysis reveals a multitude of vegetation changes behind this trend: shrubification, increased growth, increased leaf area, phenological shifts, and changes in species composition (Bjorkman et al., 2020; Mod and Luoto, 2016; Myers-Smith et al., 2020). Simultaneously, browning trends have resulted from permafrost thaw, fires, herbivory and erosion (Bjerke et al., 2017; Myers-Smith et al., 2020; Treharne et al., 2019).

Arctic remote sensing is challenging due to vegetation characteristics, geography and weather. The Arctic is characterised by treeless tundra of high fine-scale spatial heterogeneity (Dobbert et al., 2021; Reichle et al., 2018; Virtanen and Ek, 2014). This spatial diversity complicates measurements and models of, for instance, the carbon cycle in tundra (Tuovinen et al., 2019), but also remote sensing of vegetation properties. In spatially heterogeneous tundra landscapes, uncrewed aerial vehicles (UAVs) with ultra-high spatial resolution enable the observation of vegetation phenological changes and ecosystem processes that are not adequately captured using satellites (Assmann et al., 2020; Beamish et al., 2020; Danby, 2011; Poley and McDermid, 2020; Yang et al., 2021). Furthermore, at high latitudes, cloud cover and low solar angles complicate the use of satellite information (Nelson et al., 2022). Thus, aerial – whether crewed or uncrewed – imaging is a valid option, even more so with the proliferation of UAVs, with established applications in various ecosystems (Näsi, 2021; Räsänen et al., 2020b). Moreover, the absence of tree cover allows for the visibility of the ground and field layers, and relatively low species richness reduces the complexity of community composition, making it possible to apply close-range remote sensing data in tundra ecosystems. Feasible ecological applications include tracking vegetation change and modelling the spatial distribution of vegetation characteristics, such as community composition, leaf-area index (LAI), aboveground biomass (AGB) and photosynthetic capacity through biophysical traits and leaf nutrient content (Beamish et al., 2020; Danby, 2011; Nelson et al., 2022; Poley and McDermid, 2020; Räsänen and Virtanen, 2019; Yang et al., 2021).

In the Arctic, productivity and carbon storage metrics AGB and LAI are the most common vegetation parameters estimated with remote sensing data (Bartsch et al., 2020; Bratsch et al., 2017; Chang et al., 2022; Erlandsson et al., 2022; Halme et al., 2019; Orndahl et al., 2022; Pang et al., 2022; Räsänen et al., 2019a, 2020b). Vegetation structure properties such as plant functional type (PFT), biodiversity or community composition are also relatively well studied (Feilhauer et al., 2021; Kupková et al., 2023; McPartland et al., 2019; Rapinel et al., 2018). While broadband multispectral imaging (MSI) tends to outperform hyperspectral imaging in estimating productivity metrics (Broge and Leblanc, 2001; Halme et al., 2019; Poley and McDermid, 2020), the proliferation of lightweight HSI sensors offers potential for improvements in mapping vegetation diversity and composition (Fassnacht et al., 2022; McPartland et al., 2019).

Close-range HSI has evolved as an intermediate method between satellite sensors and hand-held spectrometers but its use has also introduced new challenges. The continuously changing, layered, and overlapping mosaic of species in landscapes constrains the practical differentiability of vegetation patterns, and a high spatial resolution means that highly local and variable features such as shadows have a significant influence on spectral response (Adão et al., 2017; Banerjee et al., 2020), even more so in the Arctic where tree canopy cover is intermittent at best. Assmann et al. (2019) identified differences among sensors and sensor units, changes in ambient light (weather and position of sun), and spatially constraining the imagery as three main sources of error in UAV MSI, and these can be generalised to UAV HSI as well. Moreover, HSI data processing procedures differ from MSI and are markedly more complex, and thus more labourious and more error-prone (Nex et al., 2022). In principle, however, HSI should deliver everything MSI does and more.

Arctic studies in close-range HSI have explored various vegetation and environmental properties, but results are somewhat contradictory, depending on the specific properties being examined. In a large-scale look at tundra, Nelson et al. (2022) demonstrated high spectral diversity over relatively small scales, indicating potential utility for HSI in differentiating between vegetation at close range. Liu et al. (2017) showed that narrowband HSI vegetation indices (VIs) slightly outperformed broadband MSI VIs in estimating green cover in a High Arctic mostly mesic tundra. In alpine grassland tundra, Kupková et al. (2023) demonstrated high performance for estimating dominant species cover by both MSI and HSI at ultra-high resolutions, with no performance improvement from HSI. In Arctic peatlands, Räsänen et al. (2020b) employed 28 hyperspectral bands and reported their limited added value when predicting AGB, LAI, and PFTs, while McPartland et al. (2019) found high utility in HSI for mapping functional composition and species diversity. Turner et al. (2019) found that an ideal sensor for mapping Antarctic moss cover would be a hyperspectral sensor with 25 visible and NIR bands. These examples demonstrate the heterogeneity of tundra systems and the non-universality of optimal remote sensing applications and thus the need to examine the applicability of HSI solutions in specific contexts. Thus, here, we examine the potential of HSI to improve the predictability of shrub heath tundra vegetation community properties – in particular, productivity metrics AGB and LAI, biodiversity metrics and community composition – relative to broadband MSI acquired with UAVs.

Globally, research has indicated that broadband VIs that utilize near-infrared (NIR, 700–1300 nm) reflectance (Huete, 2012) are closely correlated with AGB and LAI (Cunliffe et al., 2022; Sundqvist et al., 2020). Indeed, HSI has typically not been found to add value to productivity estimation (Broge and Leblanc, 2001; Halme et al., 2019). However, the NIR VI–productivity relationship has been disputed in the tundra, where the degrees of correlations depend on the specific plant composition (Cunliffe et al., 2020; Räsänen et al., 2021b). Instead of using spectral data, some studies have modelled canopy height and structure to estimate productivity parameters. For example, Cunliffe et al. (2020) reported that canopy height models (CHMs) have significantly higher predictive capability of AGB than spectral VIs in shrub tundra, a result echoed by Villoslada et al. (2023).

Regarding biodiversity, studies outside the Arctic (Madonsela et al., 2017; McPartland et al., 2019; Palmer et al., 2002; Rocchini et al., 2010) have suggested that spectral diversity correlates with species diversity, though the validity of this spectral diversity hypothesis has been questioned (Fassnacht et al., 2022; Wang and Gamon, 2019). Nonetheless, there has been little research in the Arctic landscapes regarding the estimation of biodiversity from spectral properties.

Finally, characterizing terrestrial vegetation community composition is also a common remote sensing task. In principle and in some demonstrations, HSI can improve the estimation of vegetation composion (e.g., McPartland et al., 2019), which is also strongly dependent on topography (Haapasaari, 1988; Oksanen and Virtanen, 1995). Topography, ranging from elevation to micro- and macro-topographic features, is indeed often an important factor in successful remote-sensing-based vegetation mapping (Dobbert et al., 2021; Mekonnen et al., 2021; Villoslada et al., 2023). While discrete differentiation between vegetation types is typical both in characterization of plant communities (Haapasaari, 1988; Oksanen and Virtanen, 1995; Pääkkö et al., 2018) and in land cover mapping (Ju et al., 2005), there are intuitive and empirical reasons for the use of fuzzy classification and gradient mapping, particularly in species-poor environments (Feilhauer et al., 2021; Rapinel et al., 2018; Räsänen et al., 2020a; van der Merwe et al., 2023). Fuzzy classifications more accurately reflect the reality of plant distributions and can be readily used to create crisp classes if necessary. At the same time, the relationship between fuzzy classes and floristic gradients

on one hand, and spectral properties on the other, can be difficult to generalise due to its strong dependence on the specific classification and determination of those gradients. For example, the use of ordination axes in gradient mapping (Feilhauer et al., 2021; Räsänen et al., 2020a) makes more sense the more those ordination axes correspond to identifiable ecological properties such as moisture and nutrient availability.

Overall, understanding of the applicability and advantages of UAV HSI to detect Arctic tundra vegetation characteristics remains limited. To address this gap, we ask: (1) How does HSI impact the predictability of plant community attributes relative to MSI? (2) How does the importance of different kinds – topographic, MSI, and HSI – of explanatory data change when modelling different responses? Increased spectral information from HSI can enable better differentiation between taxa and thus better estimation of vegetation composition and diversity than MSI. However, the importance of NIR and vegetation structure for productivity estimation suggests that HSI may not provide benefits in this area. Thus, we hypothesise that hyperspectral data improve the predictabilities of tundra plant community composition and diversity attributes (species richness and Shannon's index), but not productivity metrics (AGB and LAI). We expect topographic data to be particularly important for community composition, MSI to be most important for productivity and HSI to be important for both composition and diversity.

2. Materials and methods

We used various aerial remote sensing data, including 4-band crewed aerial MSI, 5-band UAV MSI, and 112-band UAV HSI, and an aerial lidar-derived digital elevation model (DEM) to predict vascular plant productivity (AGB, LAI), biodiversity (species richness, Shannon's diversity index; Shannon, 1948), and fuzzy and discrete plant community cluster membership in an oroarctic tundra landscape in northern Finland. We combined the remote sensing data into 12 explanatory datasets to predict field-observation-based vegetation characteristics using random forest models (Fig. 1).

2.1. Research site

The research site is located on the north and east faces of Niilanpää fell in the Saariselkä fell range in the Urho Kekkonen National Park in northern Finland (68.34° N, 27.55° E; 335–485 m a.s.l.; Fig. 2). The landscape is mostly dry shrub tundra heath (characterised by evergreen shrubs such as *Empetrum nigrum* ssp. *hermaphroditum*), with occasional more moist areas (characterised by deciduous shrubs such as *Vaccinium myrtillus*) and blockfields devoid of vegetation other than crustose lichens. Towards the lower range of elevations, the landscape gradually turns into a sparse treeline forest, with occasional Scots pines (*Pinus sylvestris*) and local variants of mountain birch (*Betula pubescens* ssp. *czerepanovii* var. *appress*), which grow as tall shrubs or small trees.

2.2. Field data

Field data were collected in summers 2020 and 2022 by sampling $n = 202$ 0.5 × 0.5 m vegetation plots (Fig. 2). Field surveys were timed to correspond approximately to the peak of the growing season from mid-July to early August. In 2020, $n = 108$ plots were randomly placed around three areas within the study site and surveyed Aug 3–7. In 2022, $n = 70$ plot locations were chosen by randomly selecting locations from a grid of regularly placed points in the research area and surveyed Jul 18–21. In addition, in 2022, $n = 24$ plots were surveyed Aug 1–4 around three relatively lush vegetation areas at the south end of the study site due to the experimental setup of another study. Field data from 2020 and 2022 were combined into a single response dataset, as interannual

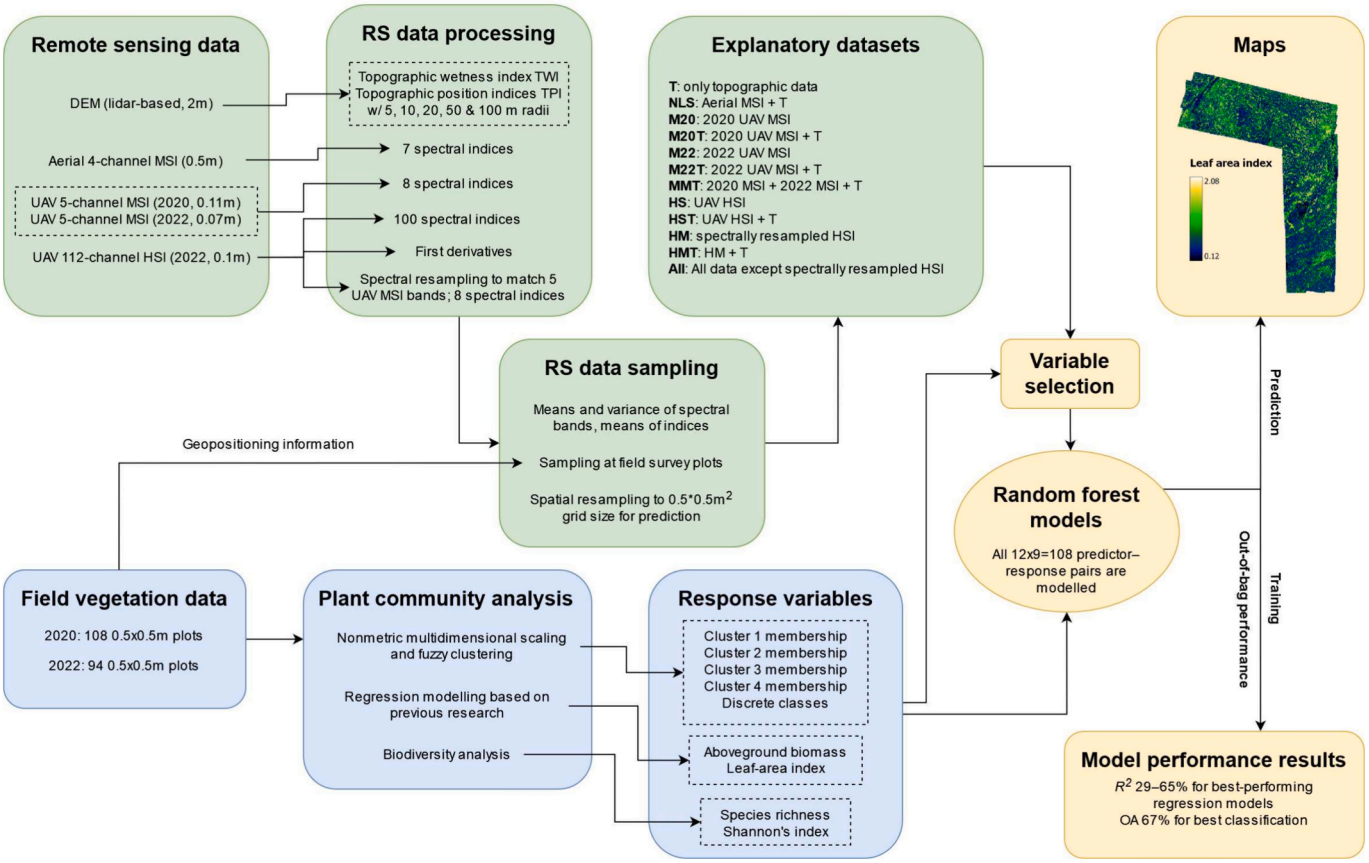

Fig. 1. Data inputs and processing steps of the models for plant community property prediction. DEM: digital elevation model; MSI: multispectral imaging; UAV: uncrewed aerial vehicle; HSI: hyperspectral imaging; RS: remote sensing.

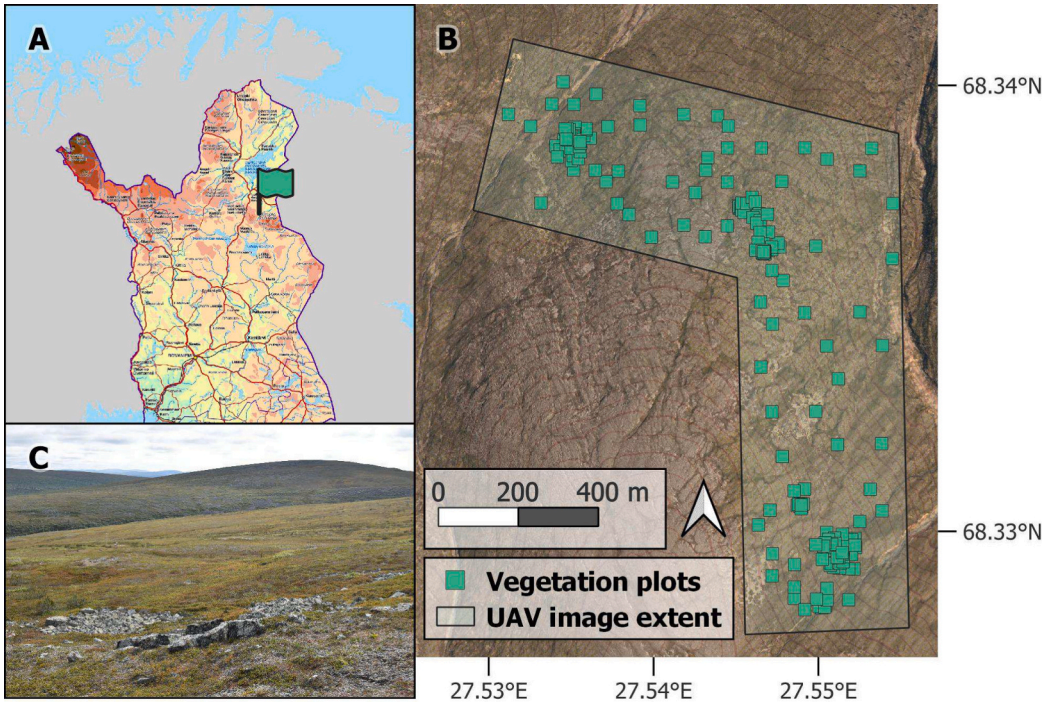

Fig. 2. A map showing the location of the study site (A), the distribution of vegetation plots and the extent of UAV imagery (B) and a landscape photo of the area (C; July 14, 2019; courtesy of T.V.). Plot sizes are not to scale. Orthophoto and topographic map are from the National Land Survey of Finland.

variability in these evergreen-perennial-dominated shrublands is small (Pääkkö et al., 2018).

Vegetation plots were aligned cardinally using a compass. Plots were photographed (Fig. 3) for later reference and the location of each plot was recorded using a Trimble R10 (Trimble, Westminster, CO, USA) GNSS RTK receiver (horizontal precision for all points < 2 cm). For each plot, vascular plant, moss, and lichen species were identified, their %-cover was visually estimated, and the mean height of vascular plants was measured with a ruler. Bryophytes and lichens were not consistently identified to species level and were later grouped into three categories: bryophytes, reindeer lichens, and other lichens. To ensure consistency, part of the field surveyers were present both in the 2020 and 2022 campaigns.

From %-cover and height information, vascular plant AGB and LAI were estimated using regression equations by plant functional type (PFT; Table 1). This approach, which has been employed in similar lanscapes previously (Räsänen et al., 2019a, 2020b, 2021b) and has the benefit of reducing the amount of field work required, but as any regression model, underestimates the true variance in AGB and LAI patterns. For this study, we curated a selection of field samples from three previous field campaigns in treeless environments in Northern Finland and selected the best-performing linear regression models, based on root-mean-square error. For many of the PFTs, AGB and LAI estimates relied solely on %-cover information, likely due to the homogenous low height of vegetation. While this means that AGB and LAI estimates are close to being linear combinations of %-cover information, they are preferable metrics from an ecological mapping point of view, as they have direct relevance to, for example, the carbon cycle (Turner et al., 2004). Bryophytes and lichens were excluded from these estimations due to their relatively low visibility below other vegetation layers and low prediction accuracy in regression models (Räsänen et al., 2020b).

Vascular plant biodiversity was quantified using species richness S and Shannon's diversity index H (Shannon, 1948). S (i.e., the number of vascular plant species present in each plot) was directly extracted from field observations, and H was calculated as:

$$H = -\sum p_i ln(p_i),$$

where

$$p_i = \frac{C_i}{C_t},$$

where C_i and C_t were species coverage and total coverage in the plot, respectively.

Vegetation was also divided into fuzzy community clusters in an unsupervised process by: 1) non-metric multidimensional scaling into four floristic gradients based on Bray-Curtis dissimilarity using the `vegan` package in R (Bray and Curtis, 1957; Minchin, 1987; Oksanen et al., 2022; R Core Team, 2021); and 2) fuzzy k-medoids with noise clustering using the `fclust` package (Ferraro Brigida et al., 2019). The number of clusters k was determined based on cluster validity indices for 2–10 clusters and by qualitatively examining the species composition in each cluster and assessing whether the results corresponded with field experiences. The result of fuzzy clustering for each resulting cluster was a cluster membership value ($\mu_k \in [0, 1]$, where $\sum_{k=1}^{4} \mu_k = 1$), as well as a discrete cluster assignment, based on highest membership value. Intuitively, fuzzy clustering corresponds more closely to real plant communities than discrete clustering since clusters can co-occur, in addition to which it has been found to improve mapping accuracy (Feilhauer et al., 2021; Rapinel et al., 2018).

2.3. Remote sensing data

Remote sensing data consisted of spectral and elevation data produced by the National Land Survey of Finland (NLS) and data collected with UAVs. Spectral data were divided into three categories: 1) 4-band moderate-altitude aerial orthophotos, which are available across Finland, produced by the NLS; 2) 5-band UAV MSI; and 3) 112-band UAV HSI. Additionally, elevation data from the NLS (lidar-based raster with 2 m resolution, measured for the study area on June 28, 2011) were used.

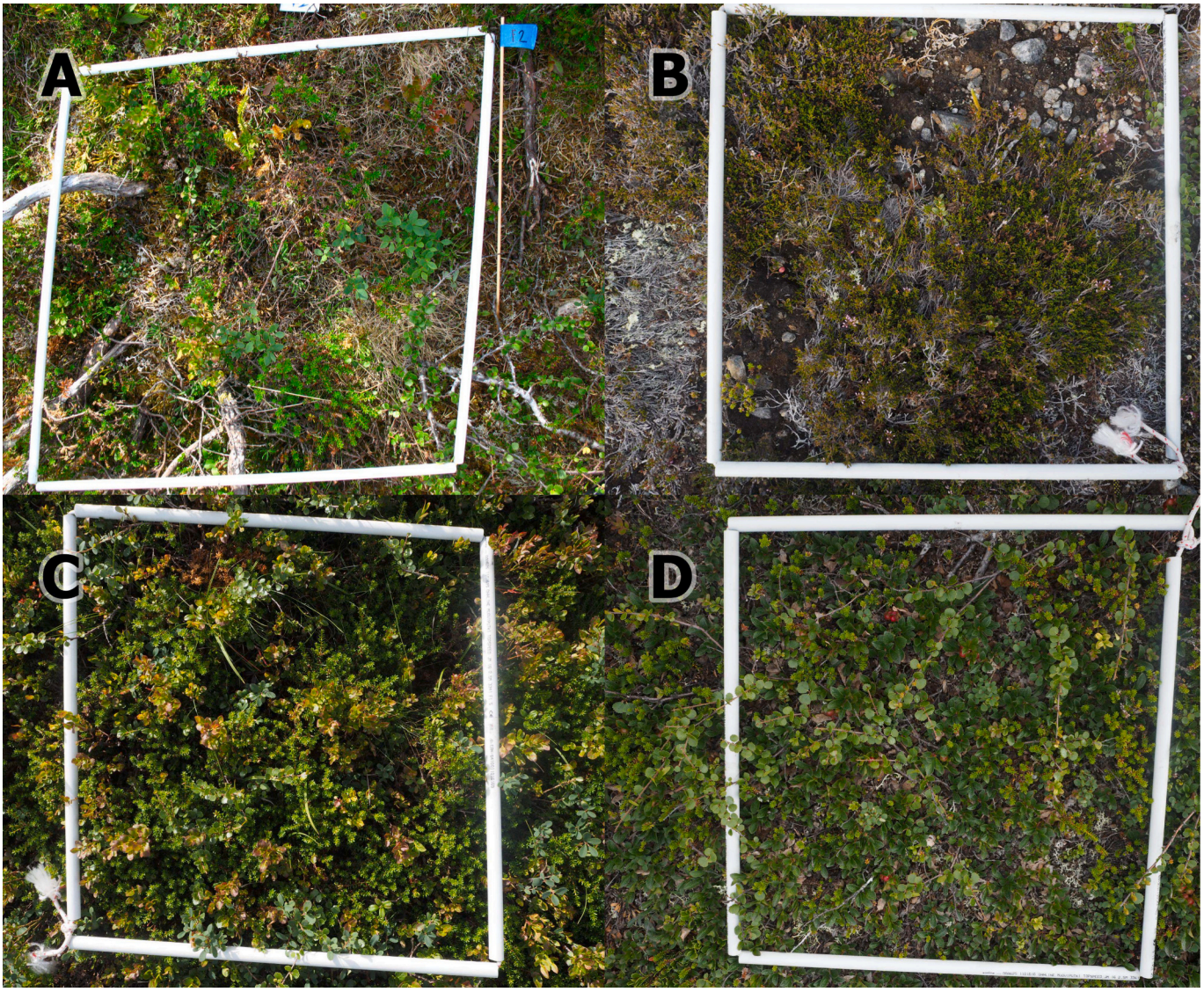

Fig. 3. Images of four vegetation plots, showing different vegetation in the study area and the dominant species. The plots represent A) a moist site, with *Vaccinium uliginosum* and graminoid species (Aug 4, 2020); B) a dry, *Calluna vulgaris*-dominated rocky site (Jul 19, 2022); C) a relatively moist and nutrient-rich site, with relatively tall specimen of *Vaccinium myrtillus* and lush *Empetrum nigrum* ssp. *hermaphroditum* (Jul 19, 2022); D) a somewhat dry site, characterised by *Betula nana* and *Arctous alpina* (Jul 19, 2022).

NLS imagery included red, green, blue and NIR bands and had a pixel size of 0.5×0.5 m^2. The most recent images for the studied area were taken on July 23, 2016. The NLS produces 4-band orthophotos across Finland at regular intervals and we used the most recent imagery for our site. The sensor, imaging, and processing details are not published (National Land Survey of Finland, n.d). Although these kinds of images are processed for visual interpretation, not reflectance measurement, they have been found to have validity in index-based computational productivity assessment (Erlandsson et al., 2019).

UAV multispectral imaging (MSI) was conducted in 2020 (August 3) and 2022 (July 21), using the MicaSense RedEdge-M and MicaSense RedEdge-MX sensors (AgEagle Aerial Systems Inc., Wichita, KS, USA), respectively. MSI consisted of 5 bands: blue, green, red, red edge and near infrared with the same central wavelengths but slightly different bandwidths (Table 2). Radiometric calibration for MSI was undertaken using a Micasense Calibrated Reflectance Panel with known reflectance (blue = 46.97%, green = 47.18%, red = 47.21%, red edge = 47.20%. NIR = 47.12%). Before and after each flight, an image of the reflectance panel was taken. Further, a Downwelling Light Sensor (DLS 2) placed on top of the UAV was used to record sun irradiance and sun angle for each of the five bands. The information from the calibration panel and the DLS2 sensor was used in Agisoft Metashape 1.7.2. (Agisoft LLC, St. Petersburg, Russia) to radiometrically correct the multispectral mosaics and account for variations in light conditions during the flights. In 2020, flight altitude was constant above takeoff, leading to real altitudes of ca. 60–200 m and ground sampling distances (GSDs) of 5–13 cm, while in 2022, altitude was constantly 100 m above terrain, with GSD 7 cm. We assumed that differences in GSD did not significantly impact the performance of these datasets, as spectral data were sampled at plots mainly as means and differences resulting from UAV imaging GSD have been found to be small (Steenvoorden et al., 2023). Georeferencing was conducted using ground control points and real-time kinematic positioning on-board UAVs, and final horizontal accuracy of mosaics was ≤ 5 cm.

UAV hyperspectral images (HSI) were collected on July 21, 2022 using a Specim AFX10 sensor (Specim, Spectral Imaging Ltd., Oulu, Finland). GSD ranged ca. 10–19 cm due to constant flying altitude above sea level and varying terrain elevation above sea level. The spectral range of the sensor was 400–1000 nm with a 5.5 nm spectral resolution. Spectral binning was set to 4 to produce 112-band images, so that the

Table 1
Equations used for estimating aboveground biomass (AGB, gm^{-2}) and leaf area index (LAI) for different functional groups of tundra plants. *C* refers to %-cover and *H* to height. Tested explanatory variable combinations were $\{C\}$, $\{CH\}$ and $\{C, H\}$ and equations were determined following methodology outlined by Räsänen et al. (2019a) on data from Finnish sites in Kaamanen (Kou et al., 2022), Pallas (Räsänen et al., 2021a) and Sodankylä (Räsänen et al., 2020b).

Plant functional type (PFT)	n	Metric	Equation	R^2	RMSE
Evergreen dwarf shrubs	103	AGB	$4.2732 + 2.75C$	0.68	36.99
		LAI	$0.0202169 + 0.0087463C$	0.74	0.10
Deciduous dwarf shrubs	46	AGB	$1.8423 + 2.4306C + 1.4118H$	0.84	20.91
		LAI	$-0.020214 + 0.0193134C$	0.76	0.17
Betula nana	45	AGB	$2.209027 + 0.160556CH$	0.73	37.98
		LAI	$0.0047927 + 0.0077365C$	0.59	0.06
Forbs & pteridophytes	73	AGB	$-0.392171 + 0.083511CH$	0.63	15.21
		LAI	$-0.01987 + 0.001125CH$	0.78	0.14
Graminoids	105	AGB	$-1.4051 + 0.6973 + 1.0906$	0.44	24.28
		LAI	$-0.015802C + 0.00585C + 0.006981H$	0.44	0.17

Table 2
MicaSense RedEdge-M and RedEdge-MX band centers and bandwidths (MicaSense, 2020).

Band	Center (nm)	RedEdge-M bandwidth (nm)	RedEdge-MX bandwidth (nm)
Blue	475	20	32
Green	560	20	27
Red	668	10	16
Red edge	717	10	12
Near infrared	842	40	57

difference between central wavelengths was 5.4 nm, close to the spectral resolution. Binning also reduced data load and processing times and improved signal-to-noise ratio. In order to compare sensor performance and in addition, HSI was spectrally resampled to correspond to RedEdge-MX bands (Table 2), assuming a Gaussian response. Resampling was performed using the `spectralResampling` function of the `hsdar` package in `R` (Lehnert et al., 2019).

For HSI, 3 radiometric calibration panels ($0.5 \times 0.5 m^2$, reflectance 2, 9, and 46%; Altisense Ltd., Pori, Finland) were placed in the landscape. Reflectance conversion was conducted with the empirical line calibration method (Fig. 4).

Image data were sampled at each field observation plot using the `exact_extract` function of the `exactextractr` package (Daniel Baston, 2023) in R. Both means and variances were extracted for each MSI and HSI band but only means for NLS airborne data, since the 0.5 m resolution corresponded with the plot size. Variances represented spectral variability in each plot to test their usefulness particularly in predicting biodiversity metrics. Additionally, seven spectral indices were calculated for NLS images, eight for MSI and spectrally resampled HSI, and 100 for HSI to reduce the complexity of multidimensional reflectance information (full descriptions and references for indices are available in Supplementary Information SI 1). For HSI, first derivatives were calculated. For MSI and spectrally resampled HSI, a limited number of common indices were chosen while, in contrast, all applicable vegetation and soil indices available in hsdar were computed for HSI. Thus, the number of explanatory variables computed from MSI was 18 while it was 435 from HSI. From the elevation model, topographic

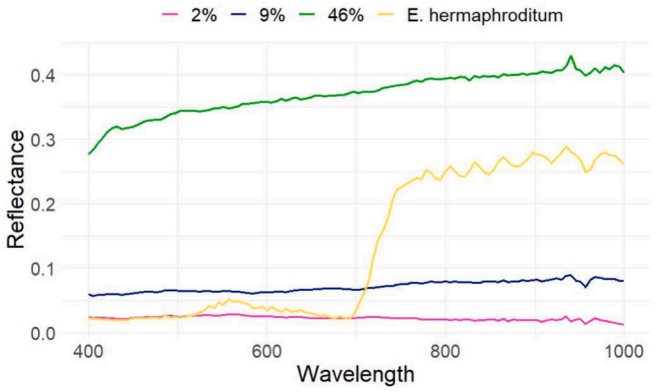

Fig. 4. Hyperspectral reflectance spectra at calibration panels (2–46%) and a typical *E.-hermaphroditum*-dominated spot in the scene. Spectra were obtained by weighted averaging over small ($< 0.2 m^2$) hand-drawn areas at selected locations.

position indices (TPI) with neighbourhood distances of 5, 10, 20, 50, and 100 m (Guisan et al., 1999) and the topographic wetness index (TWI; Böhner and Selige, 2006) were calculated using SAGA-GIS (Conrad et al., 2015).

2.4. Statistical modelling

Before model building, field and remote sensing data from different years were evaluated for compatibility based on seasonality as measured by accumulated thermal units (ATUs) and precipitation and by cross-modelling some responses (SI 5). Based on these results and our experience-based understanding and earlier evidence of small interannual variability in our study site (Pääkkö et al., 2018), the field and remote sensing data were modelled together.

To assess differences in the explanatory power of MSI and HSI, as well as the importance of topographic information, remote sensing data were compiled into 12 different explanatory datasets: 1) elevation data and derived topographic indices only (T); 2) NLS 4-band multispectral and topographic data (NLS); 3) multispectral data from 2020 (M20); 4) M20 with topographic data (M20T); 5) multispectral data from 2022 (M22); 6) M22 with topographic data (M22T); 7) two-year multitemporal multispectral data and topographic data (MMT); 8) hyperspectral data (HS); 9) HS and topographic data (HST); 10) hyperspectral data spectrally resampled to match MSI data (HM); 11) HM and topographic data (HMT); and 12) all original spectral and topographic data (All) (Table 3 for details). Datasets were compiled based on spectral and spatial resolution and the inclusion of topographic data, as well as cases,

Table 3
Explanatory datasets based on remote sensing. Dataset names beginning with M are UAV MSI, while those beginning with H are UAV HSI, and those with HM are HSI data spectrally resampled to correspond to MSI. T signifies that topographic data was included, and NLS is the National Land Survey of Finland, who produced crewed aerial orthophotos.

Name	Imaging year(s)	NLS	MSI	HSI	HM	T
T	–	–	–	–	–	×
NLS	2016	×	–	–	–	×
M20	2020	–	×	–	–	–
M20T	2020	–	×	–	–	×
M22	2022	–	×	–	–	–
M22T	2022	–	×	–	–	×
MMT	'20, '22	–	×	–	–	×
HS	2022	–	–	×	–	–
HST	2022	–	–	×	–	×
HM	2022	–	–	–	×	–
HMT	2022	–	–	–	×	×
All	'16, '20, '22	×	×	×	×	×

where data availability was limited to one type of sensor or publicly available data. Data were also combined in datasets MMT and All to assess possible benefits from multitemporal data and fusion between MSI and HSI.

Ecological metrics[1] (AGB, LAI, vascular plant species richness, Shannon's diversity index for vascular plants, and community cluster classification and membership) were estimated from these datasets using random forest machine learning models (Breiman, 2001). Random forests are considered resistant to overfitting (Breiman, 2001) and their use in remote-sensing ecology is well-established (e.g., Hall and Lara, 2022; Räsänen et al., 2020a; Turner et al., 2019). Due to the large number of derived variables, such as topographic and spectral indices, there was high redundancy in our datasets. Thus, the number of explanatory variables was reduced using `VSURF` (Genuer et al., 2015), a random-forest-based variable selection algorithm. The algorithm works by: 1) ranking variables by importance and eliminating irrelevant variables; 2) building a sequence of models with the most important, two most important, etc. variables and selecting those that construct the best model; and 3) testing different combinations of variables and choosing the least erroneous combination (Genuer et al., 2015). Since random forests employ stochastic processes, results for variable selection vary on different executions of the algorithm. Therefore, the final variable selection was based on 10 executions of the `VSURF` algorithm. While this approach is counterintuitive with regards to the redundancy-reducing process of `VSURF`, it was found in preliminary modelling runs to provide the best performance (SI 2).

In the final random forest models after `VSURF`, the random forest parameter `mtry`, which determines the number of variables randomly selected for testing the split at each node of the decision trees, was tuned using the `tuneRF` function in the `randomForest` package (Liaw and Wiener, 2002). The function first tries $\sqrt{n}$ variables, where n is the total number of variables in the model, and then iteratively increases and decreases this number, stopping in each direction when errors increase. Such a parameter value was chosen that yielded the minimum mean square error. Next, 100 random forests were built for each dataset and they were evaluated using mean values of the out-of-bag estimate of the percentage of variance explained (R^2, $R^2 = 1 - \frac{\text{mse}}{Var(y)}$, where y is the response) and range-normalised root-mean-square error (nRMSE) for regression models, and using overall accuracy (OA), fuzzy overall accuracy (fOA) and both hard and fuzzy confusion matrices (Binaghi et al., 1999) for classification models. Instead of separating the data for cross-validation, out-of-bag model metrics were used as these have been found to be valid and even conservative estimates of model performance (Clark et al., 2010). Fuzzy confusion matrix $\mathbf{X}$ values were defined as $x_{i,j} = \sum_{i=1}^{n_c}\sum_{j=1}^{n_c}(m_j|c_t = i)$, where i and j are rows and columns, respectively, n_c is the number of clusters, m is the membership value or vote share for regression and classification, respectively, and c_t is the "true" cluster for each plot.

The relative importance of variables was evaluated using an expression of increase in root-mean-square error (relative to the response mean) if the variable in question was randomly permuted. Importance values were retrieved from a final random forest built using chosen variables for each predictor-response combination. Finally, models built with dataset All were used to predict plant community characteristics across the entire imaged area, and models built with datasets M22T and HST were used to predict productivity and diversity metrics for direct comparison between MSI and HSI. For prediction, image and topographic data were resampled to a 0.5×0.5 m resolution. This was necessary to calculate comparable spectral variance to the training data, in addition to which it reduced computational costs in prediction significantly and corresponded to the size of vegetation plots.

[1] On vocabulary: we describe response variables as *metrics* and explanatory variables as variables for clarity.

3. Results

3.1. Plant community properties

A total of 37 vascular plant species were identified, along with 26 bryophyte taxa and 30 lichen taxa. The most common species were *Empetrum nigrum* ssp. *hermaphroditum*, *Vaccinium vitis-idaea*, *V. myrtillus*, *Betula nana*, and *Calluna vulgaris*, of which all but *V. vitis-idaea* were dominant species in their respective communities (Table 4). *V. vitis-idaea* occurred almost universally but as very small individual plants (mean height 3.3 cm and mean %-cover 3.4% of a vegetation plot). Quantitative descriptions of the species (SI 3) showed how some (*E. hermaphroditum* and *V. vitis-idaea*) were universally present, while others (*B. nana*, *C. vulgaris*, *V. uliginosum*, and *B. pubescens* in particular) appeared only occasionally but had relatively high abundance when they did. Mean vegetation height across all plots was 6 cm.

Based on non-metric multidimensional scaling and fuzzy clustering, four plant community clusters were defined (Table 4; Fig. S.1). In a qualitative assessment of the discretised clusters, 1 and 2 were wetter, containing more bryophytes as well as graminoids and *V. uliginosum* and *myrtillus*. Meanwhile, clusters 3 and 4 encompassed more plots, and were characterised by *E. nigrum* and lichens, and *C. vulgaris*, respectively. Discretised clusters were also differentiated to varying extents by AGB, LAI, and biodiversity metrics. These properties were quite normally distributed overall, with variation across the clusters (Fig. 5). Clusters 2 and 3 had distinctly high and low biodiversity, respectively, while 1 and 4 had similar medium biodiversity values. AGB and LAI were the lowest in cluster 3 and the highest in cluster 4. In other respects, the clusters were less differentiable. The fuzzy nature of clustering blurred lines between the different clusters, not just in terms of cluster membership but other characteristics as well.

3.2. Remote sensing models

Model performance varied greatly across responses (R^2 0.29–0.65 for the best-performing dataset All) and across datasets (R^2 0.00–0.65 for the best-performing response LAI; Table 5). Best performing data were generally – with exceptions – fusions of multiple image and topographic data. Generally, topographic data increased performance more for MSI than for HSI, and without topographic data HSI outperformed MSI for almost all metrics, and with topographic data performance was, on the whole, approximately equal. Multitemporality slightly improved MSI performance (dataset MMT), especially for biodiversity metrics. Variable selection results agreed with these results (Table 6 for fusion dataset All, SI 2 for others), showing that MSI, HSI and topographic data were all important for some responses, though the relationship between predictor and response varied from seemingly linear to more complex (SI 7).

Better performing models exhibited less noise and their regression line slopes were closer to 1 in the predicted-observed plots (Fig. 6 for dataset All, SI 8 for others). These plots also show that cluster membership models are generally more noisy than productivity or biodiversity models, as shown in generally larger error values.

3.2.1. AGB and LAI

The best regression model performance was achieved for LAI with dataset All, yielding R^2 0.65 and nRMSE 0.09 (Table 5). For productivity metrics AGB and LAI, all MSI and HSI datasets performed similarly ($R^2 > 0.5$), with the exception of spectrally resampled HSI, which underperformed relative to MSI. There was only a limited benefit from the inclusion of topographic data, and limited or no benefits from multitemporal or multisensor data fusion. Topographic data alone performed poorly ($R^2 \leq 0.14$), as did lower-spatial-resolution aerial MSI ($R^2 \leq 0.22$). Model performances were echoed in variable selection results (Table 6).

Table 4
Properties of plant community clusters as defined when plots were assigned to clusters for which they had the highest membership value. By a qualitative assessment of clustering, cluster 1 corresponded to the most moist and lush areas in the landscape, and cluster 2 was somewhat drier. Cluster 3 was the most common, and included the most commonly occurring species, *Empetrum nigrum ssp. hermaphroditum* and *Vaccinium vitis-idaea*. Cluster 4 was quite clearly demarcated by *Calluna vulgaris*, which was consistent with field observations. AGB: aboveground biomass; LAI: leaf area index; *S*: species richness; *H*: Shannon's diversity index. AGB, LAI, *H* and height are reported with standard deviation.

ID	Indicators	Plots	Mean AGB (g)	Mean LAI	Median *S*	Mean *H*	Mean height (cm)
1	*V. uliginosum*, bryophytes	40	180 ± 83	0.82 ± 0.43	6	1.14 ± 0.34	6 ± 5
2	*V. myrtillus*, *A. flexuosa*, *B. nana*	32	170 ± 57	0.75 ± 0.28	8	1.56 ± 0.25	6 ± 3
3	Lichens, reindeer lichens, *E. hermaphroditum*, *V. vitis-idaea*	77	153 ± 81	0.66 ± 0.41	4	0.83 ± 0.31	5 ± 6
4	*C. vulgaris*	53	216 ± 58	0.88 ± 0.29	6	1.14 ± 0.35	6 ± 4

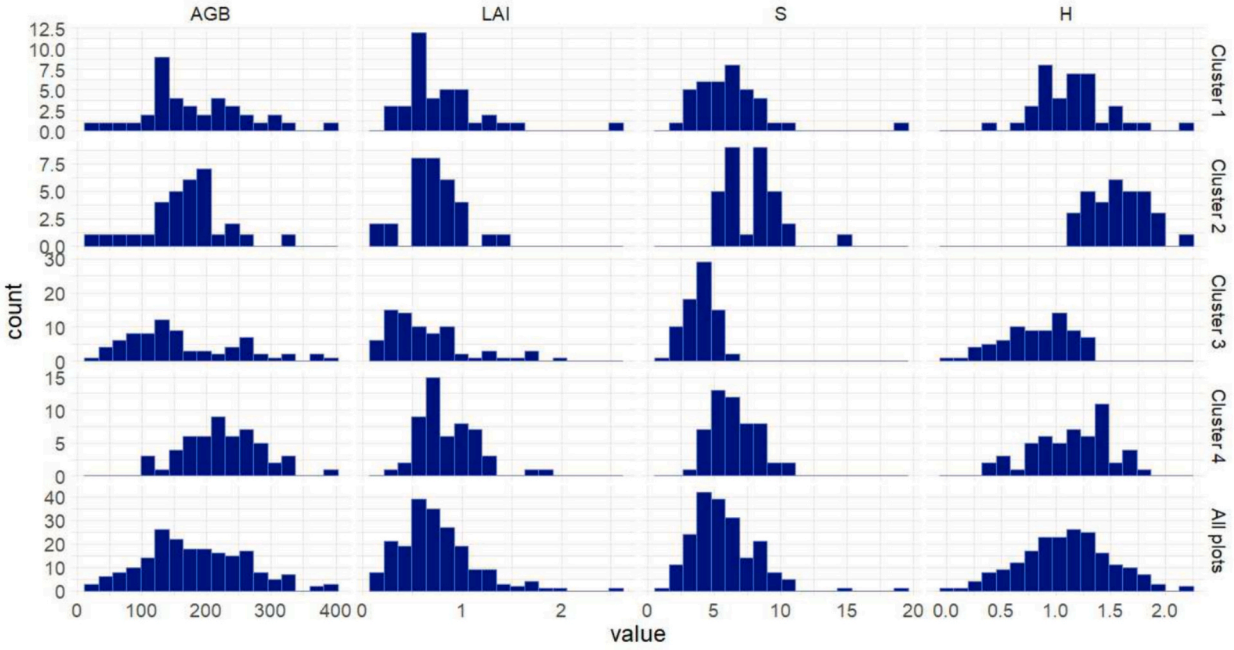

Fig. 5. Aboveground biomass (AGB), leaf area index (LAI), vascular plant species richness (S), and Shannon's diversity index (H) distributions across plots. On the bottom row are all plots, and on four other rows, those plots most likely to belong to each of four community clusters. AGB and LAI are determined according to models detailed in Table 1. Clusters 1–4 are described in Table 4.

3.2.2. *Biodiversity metrics*

Biodiversity metrics *S* and *H* were both best estimated with multi-temporal MSI and topographic data (R^2 0.53 and 0.46, respectively). One-off MSI and HSI performed similarly, though again spectrally resampled datasets HM and HMT underperformed, though only slightly for *S*. Topographic data were important, boosting R^2 values by 0.03–0.26. Notably, topographic data provided the smallest boost for HSI, and HS was the best-performing dataset without topographic data (R^2 0.46 and 0.36, respectively).

3.2.3. *Cluster membership and classification*

Community cluster classification and membership regression models had mixed results (for a comparison of community cluster classification and cluster membership regression, see SI 9). For C1 membership, HSI provided the largest boost in model performance with R^2 0.1 greater than the best-performing MSI dataset, but model performance was overall very low, peaking at 0.29 for datasets HST and All. For C2 and C3, fusion datasets performed best, and performance was better throughout than for C1. HST performed best for C4. For all cluster membership regression models, topographic information boosted R^2 by 0.02–0.35, and topography-only models often outperformed pure spectral models, particularly MSI models. HS was universally the best-performing topography-exclusive model. In classification models, fusion datasets performed best, with maximum overall accuracy 0.67, though maximum fuzzy OA was only 0.53.

Classification performance was further evaluated with hard and fuzzy confusion matrices (Tables 7–8, SI 10). In the fuzzy confusion matrix, the numbers represent the summed proportion of votes in the random forest given to each observed class. Especially fuzzy classification accuracy was poor (<0.4) for clusters 1 and 2, while clusters 3 and 4 were better predicted. The fuzzy confusion matrix reveals, for example, that plots in cluster 3 were often given high membership in C1, which was the main cause of low user's accuracy for C1.

3.3. *Prediction maps*

In the vegetation characteristic maps constructed with dataset All (Fig. 7), AGB and LAI showed the largest spatial variance and were closely positively correlated (Pearson correlation coefficient PCC 0.91, Table 9). *S* and *H* had less spatial variance and also clearly correlated with each other (PCC 0.66). Regarding community clusters, the best-predicted cluster C3 dominated the study site, with gaps being filled by C1 and C4. The maps of the wettest clusters C1 and C2 correlated with the productivity and biodiversity metric maps, as did the *Calluna*-dominated cluster 4 maps. Regression- and classification-based cluster maps had clear differences: less pixels were classified into cluster 2 in the classification map and more to cluster 4; classifier voting maps showed the benefits of classifier-based fuzzy membership by exhibiting greater

Table 5
Performance metrics for all models, with the best performing model bolded for each metric. Explanatory datasets (Table 3) are on the vertical axis while modelled metrics are on the horizontal axis. R^2 is variance explained, nRMSE is range-normalised root-mean-square error, OA is overall classification accuracy, and fOA is fuzzy overall accuracy. In dataset names: T: topographic data; NLS: data produced by the National Land Survey, including 4-band aerial orthophotos and topographic data; M: UAV MSI from 2020, 2022, or both (MM); HS: UAV HSI; HM: UAV HSI spectrally resampled to correspond to UAV MSI; All: all data.Response metrics: AGB: aboveground biomass; LAI: leaf area index; S: vascular plant species richness; H: Shannon's entropy for vascular plants; C1–C4: fuzzy community cluster membership for clusters 1–4; Class: community cluster classification.

	AGB		LAI		S		H		C1		C2		C3		C4		Class		Mean	
Dataset	R^2	nRMSE	R^2	nRMSE	R^2	nRMSE	R^2	nRMSE	R^2	nRMSE	R^2	nRMSE	R^2	nRMSE	R^2	nRMSE	OA	fOA	R^2	nRMSE
T	0.14	0.20	0.00	0.15	0.38	0.11	0.24	0.16	0.17	0.18	0.34	0.14	0.42	0.26	0.32	0.18	0.59	0.42	0.25	0.17
NLS	0.22	0.19	0.01	0.15	0.42	0.11	0.26	0.16	0.17	0.18	0.29	0.15	0.41	0.26	0.32	0.18	0.64	0.50	0.26	0.17
M20	0.53	0.15	0.56	0.10	0.39	0.11	0.26	0.16	0.10	0.18	0.24	0.16	0.37	0.27	0.26	0.19	0.62	0.46	0.34	0.16
M20T	**0.60**	**0.13**	0.57	0.10	0.49	0.10	0.41	0.14	0.19	0.17	0.34	0.14	0.50	0.24	0.43	0.17	0.63	0.48	0.44	0.15
M22	0.52	0.15	0.63	0.09	0.23	0.12	0.27	0.16	0.07	0.19	0.19	0.16	0.28	0.29	0.18	0.20	0.54	0.35	0.30	0.17
M22T	0.54	0.14	0.63	0.09	0.49	0.10	0.37	0.15	0.17	0.18	0.38	0.14	0.49	0.24	0.34	0.18	0.65	0.50	0.43	0.15
MMT	0.56	0.14	0.63	0.09	**0.53**	**0.09**	**0.46**	**0.14**	0.16	0.18	0.35	0.14	0.50	0.24	0.43	0.17	0.66	0.53	0.45	0.15
HS	0.54	0.14	0.55	0.10	0.46	0.10	0.36	0.15	0.27	0.17	0.38	0.14	0.39	0.26	0.34	0.18	0.58	0.41	0.41	0.16
HST	0.54	0.14	0.55	0.10	0.49	0.10	0.39	0.14	**0.29**	**0.16**	0.40	0.14	0.50	0.24	**0.45**	**0.16**	0.63	0.48	0.45	0.15
HM	0.38	0.17	0.46	0.11	0.33	0.11	0.22	0.16	0.04	0.19	0.26	0.15	0.13	0.31	−0.03	0.22	0.46	0.24	0.22	0.18
HMT	0.42	0.16	0.47	0.11	0.47	0.10	0.33	0.15	0.18	0.18	0.38	0.14	0.47	0.24	0.32	0.18	0.65	0.50	0.38	0.16
All	0.59	0.14	**0.65**	**0.09**	0.50	0.10	0.43	0.14	0.29	0.16	**0.44**	**0.13**	**0.53**	**0.23**	0.44	**0.16**	**0.67**	**0.54**	**0.48**	**0.14**

variance and contrast relative regression membership; and the classifier maps were less "noisy" in the sense of containing larger homogenous areas. However, though these maps were neater, there was no evidence that they corresponded more accurately with the vegetation on ground – indeed, for estimating the floristically determined cluster membership, regression models outperformed classification vote shares (Tables 5, S.18). In the maps for C2 and AGB, there were some no-data pixels, which were caused by a bug producing no-data values in the calculation of the modified red edge inflection point (mREIP) raster from HSI. Since no-data values were only present in the mREIP map of the entire area, and not in training data, this issue was deemed aesthetic and ignored.

When comparing maps produced by MSI and HSI (topographic data included; Fig. 8), differences between predicted AGB and LAI were small, though MSI exhibited more variance through higher highs and lower lows, whereas more pronounced differences can be seen in *S* and *H* maps. In particular, the M22T species richness map (selected variables Ratio22, DEM and TPI-50) showed large dependence on elevation, which rises towards the south-west corner in these maps, an effect which was likely overfitted, since the relationship between elevation and species richness in this site was non-obvious (Fig. S.4). The HST species richness model had more explanatory variables than M22T species richness models; therefore, though elevation was included as a predictor in the HST model, the model was more robust for species richness and the elevation effect could not be seen. Even so, model performance metrics were the same for species richness for M22T and HST. For Shannon's index, the M22T map again showed greater variance, though model performance was 2 pp. better for HST.

4. Discussion

Based on our results, HSI improves the predictability of some tundra plant community characteristics relative to MSI. However, when topographic data are included, there is little difference in the performance between HSI- and MSI-based models. An exception in this trend are community cluster membership regressions for clusters 1, 2 and 4, where HSI and topography models have 10, 2 and 2 percentage points (pp) higher R^2, respectively, and 1 pp. lower nRMSE than MSI and topography models. Further, fusion models – combining HSI with multitemporal MSI and topographic data – boost R^2 for LAI, C2 and C3 by 2, 4 and 3 pp., respectively. While topographic data close much of the performance gap between MSI and HSI, this does not mean that spectral data can be replaced by topographic data, because topographic and spectral data provide very different information about the landscape. Our results indicate that the choice of imaging system and plan should depend on the modelled plant community property; while MSI is better for productivity estimation, HSI brings some improvements for predicting composition. Our results also suggest some benefits from including multitemporal data in estimating vegetation diversity.

In prediction maps based on random forests, spatial variation of response metrics is underrepresented, which can be seen in regression lines in observed–predicted plots (Fig. 6, SI 8). As a result, predicted metrics tend towards the mean and outliers of, for example, high or low AGB are not represented. At landscape scale, the loss of extreme values has no effect on calculated means or sums, and in maps produced by better-defined models exhibit more spatial variation (e.g. AGB and LAI maps produced by MSI vs HSI in Fig. 8).

Across responses and datasets, our results are slightly limited by spatial uncertainty and temporal mismatches. While georeferencing precision for our data was high (<5 cm), polygon representations of field plots did not exactly match surveyed plots. These issues are limitations of the technology at our disposal, but their effects on our results were likely small, as vegetation plots were not placed at stark borders between vegetation types. Moreover, while we used two MSI datasets from different years, we only had HSI for one year. Thus, the potential benefits of multiannual HSI were unexplored. In addition, MSI results showed that performance can vary with the same sensors (e.g. *S* R^2 0.39

Table 6
For each response metric, the results of 10 iterations of VSURF variable selection and importance values. Selected variables are listed in order of decreasing importance, which is expressed, for regression models, as percentage increase in MSE, if that variable is randomly permuted, normalised by the standard deviation of the difference between MSE with and without permuting. For classification, importance is mean decrease in accuracy. Spectral indices are explained and referenced in SI 1. Variable names are suffixed by NLS, 20 or 22 for National Land Survey, multispectral 2020 and multispectral 2022 images, respectively, "var" for band variance. Hyperspectral bands are named by their central wavelength prefixed by "HS", and first derivatives are suffixed by "D". Topographic data are digital elevation model (DEM), topographic wetness index (TWI) and topographic position indices (TPIs).

AGB		LAI		S		H		C1		C2		C3		C4		Class	
Variable	%	Variable	%	Variable	%	Variable	%	Variable	%	Variable	%	Variable	%	Variable	%	Variable	%
DEM	28	Ratio22	25	TPI-50	25	RE22var	25	HS1000	30	green20	22	green20	44	DEM	57	DEM	50
blue20	27	NDVI22	24	HS454D	22	TWI	22	HS984	29	greenNLS	19	DEM	34	RE20	38	green20	43
red22	27	RGI22	21	HS973D	20	DEM	21	HS984D	25	D1	18	HS903D	29	PRI_norm	36	HS454D	42
red20	26	blue22	21	HS978D	20	HS903D	19	SR8	23	RI	16	NDRE22	27	green20	32	TWI	32
NDVI22	25	red22	20	DEM	18	TPI-50	18	TPI-10	22	PRI_norm	15	PRI_norm	26			TPI-50	31
Ratio22	25	Ratio20	19	green20	17	SR3	18	HS708D	20	OSAVI2	15	HS454D	23			RE20	29
blue22	24	green22	18	HS935var	16	HS973D	18			NDRE20	15	HS978D	21				
Carter	23	NDVI20	18	blueNLS	15	SI_TM	18			HS735D	15	NIRNLS	21				
RGI20	23	RGI20	17	CRI2	15	GMI1	17			MTCI	14	D1	19				
RGI22	21	NDRE22	17	greenNLS	14	Datt3	17			HS405	14						
mREIP	21	HS400	16	Datt3	13	HS735D	15			HS903D	14						
red22var	17	RatioNLS	14	TPI-20	13	HS978D	14			MCARI2	13						
		nir22var	13	SI_TM	12					HS941D	13						
		NPCI	12	redNLS	11					MCARI2/ OSAVI2	13						
		green20	12	blue20	11					RI_TM	13						
		SRPI	12	SR8	7					HS411	13						
		PRI_norm	10							mREIP	13						
		RE20var	5							TPI-20	12						
										DD	12						
										mSR705	12						
										CI	10						

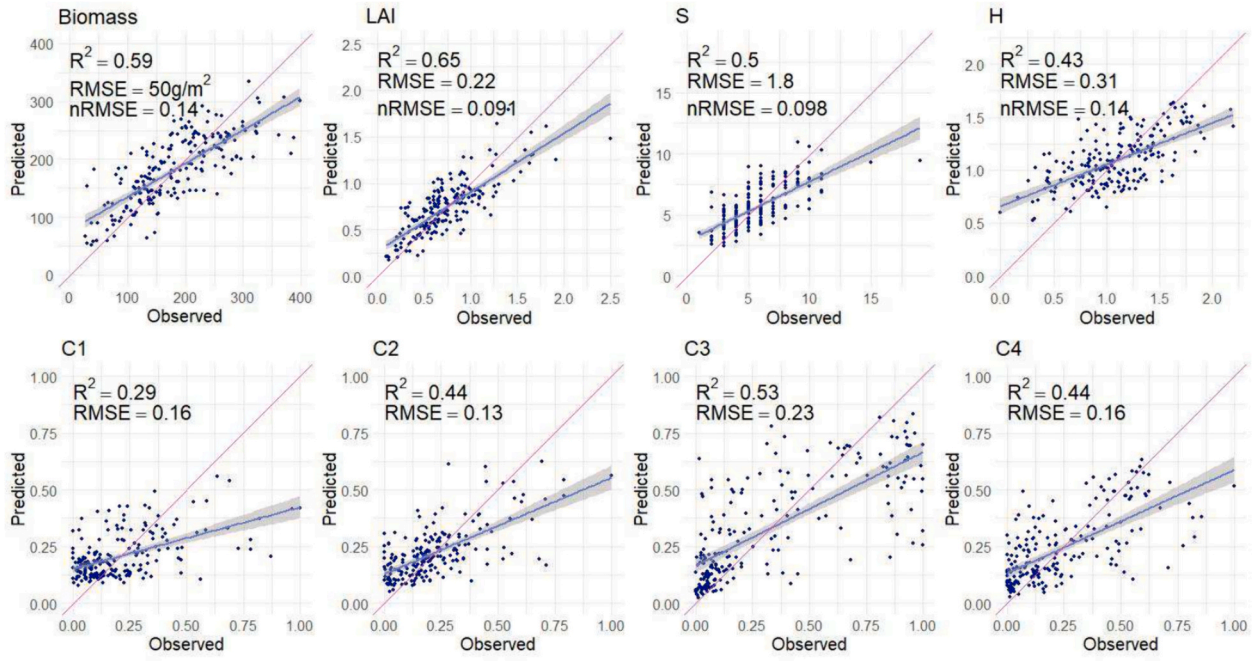

Fig. 6. Relationships between observed and predicted values for regression models built with dataset All. Linear regression estimates between predicted and observed values with confidence intervals are shown with blue coloured lines while 1:1 lines are drawn with magenta. R^2, RMSE and nRMSE values are given, though note that RMSE and nRMSE values are the same for C1–C4 since their range is 0–1. Regression slopes are consistently <1, indicating that not all variance in responses is accounted for in the models. (For interpretation of the references to colour in this figure legend, the reader is referred to the web version of this article.)

and 0.23 for M20 and M22, respectively), so it is feasible that an HSI dataset acquired at another point in time would have performed slightly differently. In the following subsections, we discuss our results in more detail and in light of previous research for our three categories of response metrics – productivity, biodiversity and community composition – separately, and then address both the limited benefits found in HSI generally and methodological limitations.

4.1. AGB and LAI

Previous studies have found that the accuracy of high-spatial resolution AGB and LAI predictions in low-growth landscapes varies

Table 7
Confusion matrix for random forest classification with dataset All. Presented numbers are averages over 100 random forest runs, and thus not whole numbers.

		Predicted				
		1	2	3	4	Producer's accuracy
Observed	1	15.23	5.78	10.87	6.12	0.40
	2	4.95	16.93	5	5.12	0.53
	3	4.93	1.00	63.99	5.08	0.85
	4	6.81	5.11	4.45	36.63	0.69
	User's accuracy	0.48	0.59	0.76	0.69	OA = 0.67

Table 8
Fuzzy confusion matrix for classification with dataset All. Presented numbers are averages over 100 random forest runs.

		Predicted				
		1	2	3	4	Producer's accuracy
Observed	1	11.49	7.17	10.86	8.48	0.3
	6.12	12.27	5.26	8.36	0.38	
	11.32	6	48.45	9.22	0.65	
	7.68	8.42	8.71	28.18	0.53	
	User's accuracy	0.31	0.36	0.66	0.52	fOA = 0.51

significantly between PFTs, study areas and used remote sensing explanatory variables. In one study, R^2 values for AGB ranged from 28% for lichens to 78% for deciduous shrubs (Orndahl et al., 2022). In between are estimates in the range 33–75% (Räsänen et al., 2019a), 36–70% (Räsänen et al., 2021b), 43–62% (Pang et al., 2022) and 50–67% (Räsänen et al., 2020b). LAI modelling performance has been similar but it has been assessed in fewer studies (Pang et al., 2022; Räsänen et al., 2020b). Results for AGB and LAI estimation when not tied to PFTs are similarly varied, with values ranging 0.60–0.90% in heath-fen tundra mosaics (Villoslada et al., 2023) and 0.31–0.65 in tussock tundra (Bratsch et al., 2017). Based on the large ranges for AGB and LAI prediction accuracy in previous studies, we assume that our models perform more accurately in some sub-areas and for some PFTs than others, depending on the vegetation and abiotic factors.

We found that MSI data were the most important for estimating AGB and LAI, though in both, HSI variables were also selected for the final models but topographic variables were not selected for LAI. Indeed, traditional greenness measures (red-green index, simple ratio, NDVI) were the most important predictors (Table 6). Recent studies indicate that accurate canopy height models could further improve these results (Cunliffe et al., 2020; Orndahl et al., 2022; Villoslada et al., 2023). Cunliffe et al. (2020), in particular, achieved remarkably high R^2 values of 90% and 92% for estimating aboveground vascular biomass with CHMs, in stark contrast to 14–23% predictions with NDVI. However, their tundra site is dominated by tall *Salix* shrubs and bushes and thus we would not expect results to directly replicate to lower-vegetation landscapes. In a later study, Cunliffe et al. (2022) applied a similar methodology to a range of sites with median R^2 of 87%. Orndahl et al. (2022), on the other hand, achieved RMSEs of 3.3–10.5 cm for plant height estimation using structure-from-motion (SfM) point clouds. In their study, the ground sampling distance (GSD) for images is < 1 cm. Noting that the vegetation in our study site is typically lower (mean dominant height ca. 6 cm) than the upper range of this error, and that our GSD was higher (7 cm at the lowest), we were unable to produce a CHM suitable for inclusion in our models (SI 11). Future research could look to develop improved methods for estimating canopy height in areas with very low vegetation.

The limited benefits of HSI data in estimating AGB and LAI that we found echoed results from Arctic peatlands (Pang et al., 2022; Räsänen et al., 2020b) and boreal forests (Halme et al., 2019). Pang et al. (2022) explored optimal spectral resampling of HSI data and found 10–20 nm to be generally most accurate for detecting peatland vegetation patterns, a bandwidth closer to those of the MSI sensors than the HSI sensor in our study. Räsänen et al. (2020b) used a HSI approach with 28 bands in the 500–900 nm range and concluded that HSI provide limited benefits. In boreal forests, Halme et al. (2019) found that high-resolution (GSD 0.7 m) HSI data performed equally (62%:63%) to lower-resolution (GSD 10 m) MSI in estimating AGB while outperfoming MSI in LAI estimation (83%:75%). The authors also argued that the increased spectral resolution is more important in improving LAI estimation than increased spatial resolution.

In our study, AGB and LAI were determined by regression models and were based on dominant height measurements and visual %-cover estimates. The subjectivity of visual estimation may increase uncertainty in estimating AGB and LAI but general biases are unlikely due to observations being made by multiple people. Regression models also underrepresent variance in AGB and LAI, and correspond to true values better in some PFTs than others (Table 1; Räsänen et al., 2019a). While this methodology also accounts for high correlations between AGB and LAI (Table 9, Fig. S.23), it is unlikely to notably change the predictive accuracy of models, though nRMSE were probably artificially low since the variance in the metric is smaller than the "real" variance (Räsänen et al., 2019a).

4.2. Biodiversity metrics

S and *H* were both best estimated by multitemporal MSI dataset MMT. That is, the best results were achieved with a dataset other than All, indicating that variable selection was unable to perform optimally with the All dataset. This may imply that repeating VSURF for variable selection leads to redundancy in explanatory variables and reduced modelling performance in some cases, as the number of selected variables for *S* from MMT was only 5 whereas 16 were selected for All, and the former obtained better results. The large number of selected variables highlights the difficulty to estimate biodiversity based on plot-level reflectance mean and variance, and spectral indices, and the relative interchangeability of many HSI indices.

HSI could hypothetically add potential to estimate biodiversity, since it can capture more subtle variations in the reflectance spectra than MSI (Carlson et al., 2007; Fassnacht et al., 2022; McPartland et al., 2019), and tundra can exhibit greater spectral diversity than MSI can capture (Nelson et al., 2022). This both does and does not bear out in our study. On the one hand, HSI variables are prevalent (8/16 and 8/12 for *S* and *H*, respectively) in selected variables from dataset All for biodiversity models. On the other hand, as noted above, the best-performing models for both metrics exclude HSI data. This finding is similar to the observation by Räsänen et al. (2020b) that even though hyperspectral data can be important according to feature selection they do not markedly improve model performance.

However, our results did indicate that HSI reduced the importance of topographic information in biodiversity estimation. While topographic information was essential for biodiversity metrics with MSI datasets (R^2 increase by ≥ 10 pp), benefits from topography were much more limited for HSI data (3 pp. in both cases). Thus, HSI did improve biodiversity estimation, but only when topographic information was unavailable. The relationship between topography and diversity is closely related to community composition, as some communities are more diverse than others (Table 4; Nelson et al., 2022; Oksanen and Virtanen, 1995; Pääkkö et al., 2018).

In addition to reflectance and first derivatives, our datasets included plot-level variances in reflectance as a measure of spectral variability, following the spectral variability hypothesis (McPartland et al., 2019; Palmer et al., 2002; Wang and Gamon, 2019). The best-performing dataset (MMT) did not utilize spectral variance variables for *S*, but for *H*, it does (Table S.13)(Table S.13), but for *H*, the best-performing model

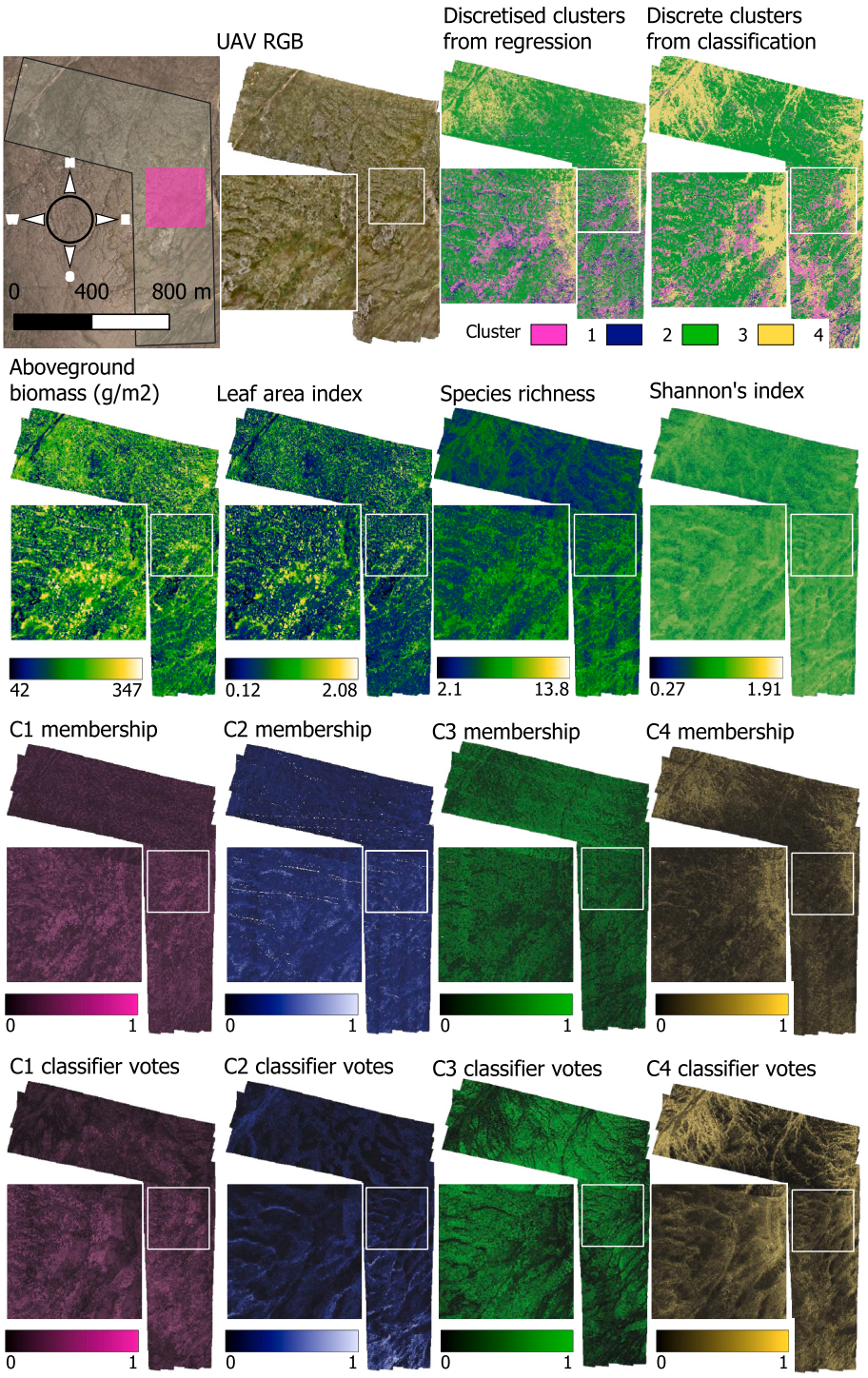

Fig. 7. Prediction maps for examined plant community metrics: aboveground biomass, leaf area index, species richness, Shannon's index and community cluster 1–4 membership values. Pictured also a general overview, UAV RGB orthomosaic (Jul 21, 2022), and two discrete clusterisations of the imaged area, the first based on cluster membership regressions and the second on random forest classification. Classifier votes are mapped in the last row.

(NMMT) does (Table S.14), though these spectral variance variables are of relatively low importance, losing to topographic and reflectance variables. In HSI models (Table S.14–S.15), only one spectral variance variable (at 935 nm in the NIR region) was selected for *S*, and none for *H*. As such, these results provide very limited support for the spectral variability hypothesis at an ultra-high spatial resolution in oroarctic tundra. In a similar vein, Fassnacht et al. (2022) have concluded that spectral variability is often subtle relative to other observable differences between taxa and the relationship between spectral and species diversity in general is unclear. However, future studies could look at the spectral diversity hypothesis in tundra landscapes across various spatial scales.

4.3. Fuzzy community clusters

4.3.1. Cluster membership regression

Model performance for fuzzy community cluster regression was mixed (R^2 0.29–0.53) and, particularly for the lowest-R^2 cluster 1, quite

Table 9
Correlation matrix for plant community characteristics: aboveground biomass, leaf area index, species richness, Shannon's index and community cluster 1–4 memberships and random forest classification vote shares. The lower left triangle contains Pearson correlation coefficients for metric values at field plots, while upper-right-triangle values are calculated across prediction maps. V1–V4 signify relative vote shares from random forest classifier.

		Across predictions											
		AGB	LAI	*S*	*H*	C1	C2	C3	C4	V1	V2	V3	V4
Across observations	AGB		0.91	0.46	0.38	0.25	0.33	−0.54	0.32	0.14	0.16	−0.38	0.27
	LAI	0.87		0.42	0.39	0.32	0.30	−0.46	0.27	0.19	0.14	−0.28	0.13
	S	0.17	0.24		0.66	0.26	0.55	−0.66	0.22	0.26	0.54	−0.59	0.25
	H	0.00	0.16	0.77		0.28	0.61	−0.65	0.20	0.21	0.49	−0.51	0.20
	C1	0.07	0.17	0.27	0.23		0.30	−0.24	−0.06	0.39	0.12	−0.13	−0.15
	C2	0.08	0.10	0.48	0.57	0.02		−0.63	0.21	0.30	0.48	−0.50	0.14
	C3	−0.25	−0.27	−0.61	−0.56	−0.45	−0.61		−0.49	−0.28	−0.40	0.72	−0.45
	C4	0.33	0.22	0.32	0.20	−0.19	0.13	−0.60		−0.22	0.09	0.53	0.69
	V1	0.03	0.19	0.23	0.17	0.40	0.00	−0.19	−0.10		0.02	−0.27	−0.26
	V2	0.10	0.14	0.47	0.45	0.13	0.51	−0.40	0.03	0.02		−0.59	−0.03
	V3	−0.32	−0.32	−0.56	−0.48	−0.19	−0.48	0.67	−0.43	−0.27	−0.59		−0.72
	V4	0.32	0.18	0.22	0.17	−0.10	0.23	−0.43	0.58	−0.26	−0.03	−0.66	

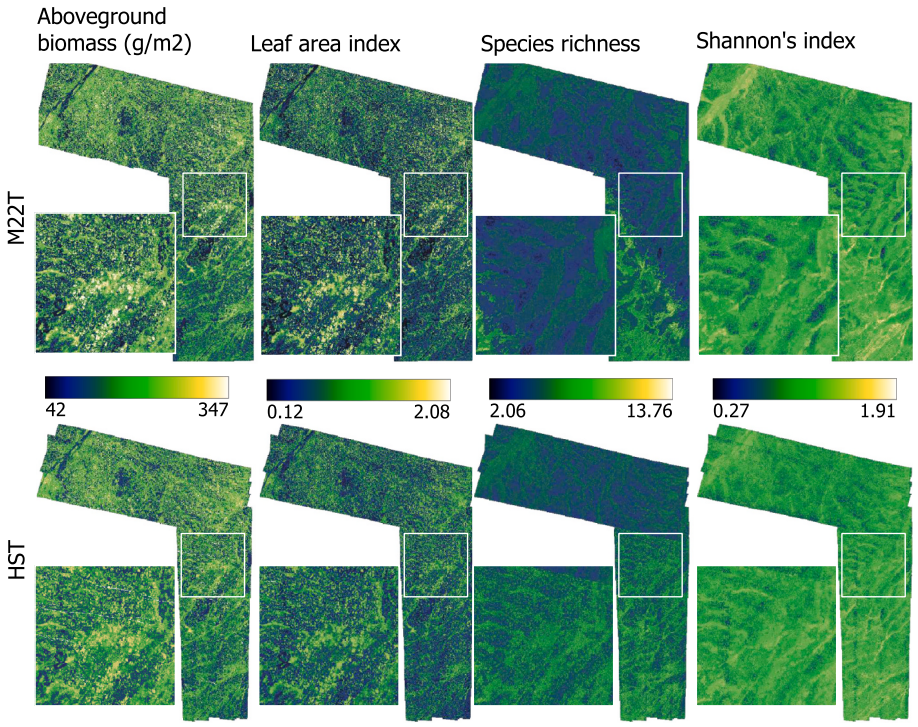

Fig. 8. Maps of productivity and biodiversity metrics produced by datasets M22T and HST; that is, by MSI and topographic data on the top row and by HSI and topographic data on the bottom.

poor. At the same time, cluster membership values for clusters 1 and 2 were the only metrics where HSI data improved results >5 pp. (10 pp. in C1 and 6 pp. when fused with MSI in dataset All for C2). Previous studies in treeless landscapes have found similarly large discrepancies in the modelling of different plant communities, with estimation accuracy ranging 0.16–0.82 in northern peatlands (Pang et al., 2022; Räsänen et al., 2019b, 2020a), 0.26–0.79 in sub-alpine peatlands (Feilhauer et al., 2021), and 0.25–0.69 in a temperate wetland (Rapinel et al., 2018). Our results fell within the lower ranges of these previous studies, but particularly good predictions were absent and most cluster membership R^2 values were under 0.5, with the exception of C3 at 0.53. Including topographic information consistently improved community cluster estimation by 2–35 pp., which corresponds to the previous determination of topography as key to community composition in tundra landscapes (Oksanen and Virtanen, 1995). As with biodiversity metrics, this improvement was smaller for HSI than for MSI. Higher spatial resolution data outperformed the lowest-resolution NLS dataset. In part, this may be explained by spectral properties, but sensor details for these images are unavailable. Finally, in the case of C1 and C2, single-year MSI datasets M20T or M22T outperformed multitemporal MSI dataset MMT, of which every variable in M22T and M20T is part by 3 pp., showing again that variable selection can notably change model performance.

Differentiation between plant community clusters must also be examined in terms of the community clusters themselves. The most poorly predicted C1 is also the most broadly defined when examined in the ordination space (Fig. S.1) and represents the wettest conditions. Conditions in the spatially limited moist areas (streambeds) in the study site differ from the dominant dry shrub heaths, but also among themselves. As a result, our data may not comprehensively represent these distinct areas within the study site and better prediction results might be obtained with a clustering based on a dataset with better representation of moist conditions. Furthermore, the strongest indicator species for C1 was *V. uliginosum*, a close relative of *V. myrtillus*, an indicator for C2,

which may have caused confusion between the two spectrally similar clusters (Lang et al., 2002). In general, however, we found that HSI improved prediction in moist areas (C1 and C2), and elsewhere, HSI has been found to be sensitive to moisture (Rehman et al., 2020). The inclusion of short-wave infrared (SWIR) data for better moisture analysis could improve these results (Kim et al., 2015; McPartland et al., 2019), though none of the available moisture indices, whether spectral or topographic, was chosen as predictors for the moist clusters in our study.

4.3.2. Cluster classification

Differences between classification models were relatively small (OA 0.46–0.67 and fOA 0.39–0.53). Topographic data alone performed better than most spectral-only datasets, with the exception of M20. Maximum OA was only 0.08 greater than topography-only OA, and fOA only 0.04 greater. There was no clear difference in performance between MSI and HSI datasets. Confusion matrices (Tables 7–8, SI 10) show that cluster 3 was predicted with notably higher accuracy than the others, and for cluster 1 both producer's and user's accuracies were below 0.5 (with dataset All).

In previous research, a common approach has been to classify tundra vegetation by dominant species: Kupková et al. (2023) classified alpine grassland tundra with accuracies of 48–100% with a similar data-fusion multispectral and hyperspectral approach as ours; Thomson et al. (2021) classified High Arctic species at 47–88% with HSI; Yang et al. (2020) classified dominant species at 46–100% in a mainly shrubby tundra setting using RGB and thermal images, and UAV-born spectrometer measurements. Our accuracies of 40–85% were slightly lower, and we did not classify by dominant species but unsupervised floristically defined clusters of co-occurent species.

4.4. Hyperspectral data

In principle, HSI data should contain all the same and more information as MSI data, particularly since the GSD was similar in our case. In a review on UAV-platform remote sensing, Nex et al. (2022) found that HSI usually outperforms MSI in complex analysis, e.g. tree species classification, and the two perform similarly when the bands that are used coincide. Why, then, did our HSI models not regularly outperform MSI ones?

One possibility is that narrowband (hyperspectral) vegetation and soil indices as employed here are not able to capture the same properties as the broadband indices. For example, when NDVI is calculated for HSI, this index uses single narrow HSI red and NIR bands, while MSI NDVI uses broad red and NIR bands that cover larger parts of the reflectance spectra. However, resampling HSI data to match MSI data did not improve performance, and both models that used spectrally resampled HSI, with and without topographic data (HM and HMT), were less accurate than those with original spectral resolution (HS and HST) for all metrics. HM and HMT models were also less accurate than single-year MSI models for all metrics except C2, where HM outperformed both M20 and M22, *S*, where HM outperformed M22, and C1, where HMT outperformed M22T. Indeed, spectral resampling may have resulted in increased noise relative to MSI while reducing informating relative to HSI. In the case where the spectrally resampled HM model outperformed single-year MSI models M20 and M22 (metric C2), this result was not repeated when topographic data was included (i.e., HMT and M22T). In spectral resampling, we assumed a Gaussian response, and while utilising a calibrated spectral response curve might have improved results, any improvements would likely have been small, since the difference in response curves is likely small (Cao et al., 2020).

Other explanations for poor HSI performance may be found in data acquisition or processing. Data processing for HSI is more complex than for MSI due to the large number of bands, pushbroom imaging technology and radiometric corrections that have to be made to obtain reflectance values (Nex et al., 2022). This means that HSI is more prone to error or processing-introduced noise, as well as being spatially less robust than MSI. Thus, benefitting from the properties of HSI relative to MSI may require optimising imaging conditions and processing pipelines. In some studies, HSI data representation is customised based on the acquired data and dimensionality is reduced based on, for example, minimum noise fractions (Hall and Lara, 2022; Kupková et al., 2023; Luo et al., 2016). Conversely, dimensionality could be further increased by computing, for example, normalised difference indices between all pairwise combinations $\binom{n}{2}$ of bands, which would add >6000 variables with our HSI. Here, in contrast, we combined bands only based on a priori spectral index definitions and to coincide with our MSI sensor, and in principle, a key benefit to random forests and other machine learning algorithms should be their ability to extract relevant information from complex data. While Hall and Lara (2022) produced encouraging results from dimension-reduced HSI, these were not reproduced by Kupková et al. (2023) who obtained approximately similar results for both UAV MSI and HSI.

Finally, hyperspectral data may better serve mapping tasks that demand a high-spectral-resolution analysis, for example estimating specific pigment content or other biochemical properties that have explicitly spectral characteristics. For example, Liu et al. (2023) recently estimated foliar photosynthetic capacity and other biochemical traits from HSI with reasonable to good results (R^2 0.38–0.6), while Peanusaha et al. (2024) estimated leaf nitrogen content with spectrometer-derived VIs with R^2 0–0.48. However, Lu et al. (2019) found only very slight benefits from hyperspectral data in estimating leaf chlorophyll content relative to VNIR MSI (R^2 0.80 vs 0.81). In Arctic contexts, biochemical traits have rarely been explicitly examined, in part due to logistical constraints (Beamish et al., 2020). Weighing these and our results, it is not obvious that HSI would perform better if response metrics were more strictly spectrally defined, but the possibility merits future research.

5. Conclusions

We conducted a unique and broad investigation on the relative utility of close-range hyperspectral and multispectral imaging as well as topographic data for mapping of natural plant communities in oroartic tundra. We showed that random forests built on close-range MSI, HSI and topographic remote sensing data estimate tundra plant community properties – AGB, LAI, species richness, Shannon's entropy, fuzzy community clusters – with moderate accuracy (R^2 0.29–0.65). Especially, AGB (0.60) and LAI (0.65) were well-estimated with multispectral datasets and traditional greenness measures. Biodiversity metrics were best estimated with multitemporal multispectral and topographic data (species richness 0.53 and Shannon's entropy 0.46). Modelling plant communities was more convoluted and some community clusters were more accurately predicted than others (R^2 0.29–0.53, classification OA 0.67). In this case, *E. nigrum* ssp. *hermaphroditum* (C3, 0.53) or *C. vulgaris* (C4, 0.45) dominated communities were modelled with the highest accuracy. These evergreen shrubs were both abundant and dominant in their respective communities, in addition to which they were found in dry areas, both factors that may have influenced estimation accuracy. Our model performance results question the utility of HSI data for these applications and assert that MSI and topographic data are often sufficient in practical applications. While HSI variables gained high importance in variable selection, this did not translate into better performance in most models that included topographic data. The exceptions were the more moist community clusters 1 and 2, which got limited (up to 10 pp) boosts from HSI data, but were also the most poorly estimated metrics. Nevertheless, when comparing models with predictors calculated only from spectral and not from topographic data, HSI typically outperformed MSI. Generally, more refined approaches in processing and representing spectral data, as well as variable selection, may lead to stronger predictions and greater advantages from HSI.

CRediT authorship contribution statement

Pauli Putkiranta: Writing – original draft, Visualization, Validation, Software, Methodology, Investigation, Formal analysis, Data curation, Conceptualization. **Aleksi Räsänen:** Writing – review & editing, Software, Methodology, Investigation, Conceptualization. **Pasi Korpelainen:** Investigation, Data curation. **Rasmus Erlandsson:** Writing – review & editing, Investigation. **Tiina H.M. Kolari:** Writing – review & editing, Investigation. **Yuwen Pang:** Writing – review & editing, Data curation. **Miguel Villoslada:** Writing – review & editing, Investigation, Data curation. **Franziska Wolff:** Writing – review & editing, Investigation. **Timo Kumpula:** Project administration, Funding acquisition, Conceptualization. **Tarmo Virtanen:** Writing – review & editing, Supervision, Project administration, Investigation, Funding acquisition, Conceptualization.

Declaration of competing interest

The authors declare that they have no known competing financial interests or personal relationships that could have appeared to influence the work reported in this paper.

Data availability

Data will be made available on request.

Acknowledgements

We thank Antti Jokelainen, Aliisa Laakkonen, Ella Romppanen, and Emelie Winquist for their assistance in collecting field data, and four anonymous reviewers for their comments which helped improve this manuscript. This work was financially supported by EU Horizon 2020 (project nr: 2020 869471) and Research Council of Finland (project nr: 330319).

Appendix A. Supplementary data

Supplementary data to this article can be found online at https://doi.org/10.1016/j.rse.2024.114175.

References

Adão, T., Hruška, J., Pádua, L., Bessa, J., Peres, E., Morais, R., Sousa, J.J., 2017. Hyperspectral imaging: a review on UAV-based sensors, data processing and applications for agriculture and forestry. Remote Sens. 9, 1110. URL. https://www.mdpi.com/2072-4292/9/11/1110. https://doi.org/10.3390/rs9111110. number: 11 Publisher: Multidisciplinary Digital Publishing Institute.

Assmann, J.J., Kerby, J.T., Cunliffe, A.M., Myers-Smith, I.H., 2019. Vegetation monitoring using multispectral sensors — best practices and lessons learned from high latitudes. J. Unmanned Vehicle Syst. 7, 54–75. https://doi.org/10.1139/juvs-2018-0018.

Assmann, J.J., Myers-Smith, I.H., Kerby, J.T., Cunliffe, A.M., Daskalova, G.N., 2020. Drone data reveal heterogeneity in tundra greenness and phenology not captured by satellites. Environ. Res. Lett. 15, 125002 https://doi.org/10.1088/1748-9326/abbf7d.

Banerjee, B.P., Raval, S., Cullen, P.J., 2020. UAV-hyperspectral imaging of spectrally complex environments. Int. J. Remote Sens. 41, 4136–4159 publisher: Taylor & Francis _eprint: https://doi.org/10.1080/01431161.2020.1714771.

Bartsch, A., Widhalm, B., Leibman, M., Ermokhina, K., Kumpula, T., Skarin, A., Wilcox, E.J., Jones, B.M., Frost, G.V., Höfler, A., Pointner, G., 2020. Feasibility of tundra vegetation height retrieval from Sentinel-1 and Sentinel-2 data. Remote Sens. Environ. 237, 111515. URL. https://www.sciencedirect.com/science/article/pii/S0034425719305346. https://doi.org/10.1016/j.rse.2019.111515.

Baston, Daniel, 2023. Exactextractr: Fast Extraction from Raster Datasets using Polygons. Https://isciences.gitlab.io/exactextractr/. https://github.com/isciences/exactextractr.

Beamish, A., Raynolds, M.K., Epstein, H., Frost, G.V., Macander, M.J., Bergstedt, H., Bartsch, A., Kruse, S., Miles, V., Tanis, C.M., Heim, B., Fuchs, M., Chabrillat, S., Shevtsova, I., Verdonen, M., Wagner, J., 2020. Recent trends and remaining challenges for optical remote sensing of Arctic tundra vegetation: a review and outlook. Remote Sens. Environ. 246, 111872 https://doi.org/10.1016/j.rse.2020.111872.

Binaghi, E., Brivio, P.A., Ghezzi, P., Rampini, A., 1999. A fuzzy set-based accuracy assessment of soft classification. Pattern Recogn. Lett. 20, 935–948. URL: https://www.sciencedirect.com/science/article/pii/S0167865599000616 https://doi.org/10.1016/S0167-8655(99)00061-6. publisher: North-Holland.

Bjerke, J.W., Treharne, R., Vikhamar-Schuler, D., Karlsen, S.R., Ravolainen, V., Bokhorst, S., Phoenix, G.K., Bochenek, Z., Tømmervik, H., 2017. Understanding the drivers of extensive plant damage in boreal and Arctic ecosystems: insights from field surveys in the aftermath of damage. Sci. Total Environ. 599-600, 1965–1976. URL. https://www.sciencedirect.com/science/article/pii/S0048969717311506. https://doi.org/10.1016/j.scitotenv.2017.05.050.

Bjorkman, A.D., García Criado, M., Myers-Smith, I.H., Ravolainen, V., Jónsdóttir, I.S., Westergaard, K.B., Lawler, J.P., Aronsson, M., Bennett, B., Gardfjell, H., Heiðmarsson, S., Stewart, L., Normand, S., 2020. Status and trends in Arctic vegetation: evidence from experimental warming and long-term monitoring. Ambio 49, 678–692. URL. https://doi.org/10.1007/s13280-019-01161-6.

Böhner, J., Selige, T., 2006. Spatial prediction of soil attributes using terrain analysis and climate regionalisation. SAGA Anal. Modell. Appl. Goltze 13–27.

Bratsch, S., Epstein, H., Buchhorn, M., Walker, D., Landes, H., 2017. Relationships between hyperspectral data and components of vegetation biomass in Low Arctic tundra communities at Ivotuk, Alaska. Environ. Res. Lett. 12, 025003. URL. https://doi.org/10.1088/1748-9326/aa572e. publisher: IOP Publishing.

Bray, J.R., Curtis, J.T., 1957. An ordination of the upland forest communities of Southern Wisconsin. Ecol. Monogr. 27, 325–349. URL. https://onlinelibrary.wiley.com/doi/abs/10.2307/1942268. https://doi.org/10.2307/1942268_eprint. https://onlinelibrary.wiley.com/doi/pdf/10.2307/1942268.

Breiman, L., 2001. Random forests. Mach. Learn. 45, 5–32. https://doi.org/10.1023/A:1010933404324.

Broge, N.H., Leblanc, E., 2001. Comparing prediction power and stability of broadband and hyperspectral vegetation indices for estimation of green leaf area index and canopy chlorophyll density. Remote Sens. Environ. 76, 156–172. Publisher: Elsevier.

Cao, H., Gu, X., Wei, X., Yu, T., Zhang, H., 2020. Lookup table approach for radiometric calibration of miniaturized multispectral camera mounted on an unmanned aerial vehicle. Remote Sens. 12, 4012. URL: https://www.mdpi.com/2072-4292/12/24/4012 https://doi.org/10.3390/rs12244012.

Carlson, K.M., Asner, G.P., Hughes, R.F., Ostertag, R., Martin, R.E., 2007. Hyperspectral remote sensing of canopy biodiversity in Hawaiian lowland rainforests. Ecosystems 10, 536–549. https://doi.org/10.1007/s10021-007-9041-z.

Chang, Q., Zwieback, S., DeVries, B., Berg, A., 2022. Application of L-band SAR for mapping tundra shrub biomass, leaf area index, and rainfall interception. Remote Sens. Environ. 268, 112747. URL: https://www.sciencedirect.com/science/article/pii/S0034425721004673 https://doi.org/10.1016/j.rse.2021.112747.

Clark, M.L., Aide, T.M., Grau, H.R., Riner, G., 2010. A scalable approach to mapping annual land cover at 250 m using MODIS time series data: a case study in the dry Chaco ecoregion of South America. Remote Sens. Environ. 114, 2816–2832. URL: https://www.sciencedirect.com/science/article/pii/S0034425710002063 https://doi.org/10.1016/j.rse.2010.07.001.

Conrad, O., Bechtel, B., Bock, M., Dietrich, H., Fischer, E., Gerlitz, L., Wehberg, J., Wichmann, V., Böhner, J., 2015. System for automated geoscientific analyses (SAGA) v. 2.1.4. Geosci. Model Dev. 8, 1991–2007. https://doi.org/10.5194/gmd-8-1991-2015.

Cunliffe, A.M., Assmann, J.J., Daskalova, G.N., Kerby, J.T., Myers-Smith, I.H., 2020. Aboveground biomass corresponds strongly with drone-derived canopy height but weakly with greenness (NDVI) in a shrub tundra landscape. Environ. Res. Lett. 15, 125004 https://doi.org/10.1088/1748-9326/aba470.

Cunliffe, A.M., Anderson, K., Boschetti, F., Brazier, R.E., Graham, H.A., Myers-Smith, I.H., Astor, T., Boer, M.M., Calvo, L.G., Clark, P.E., Cramer, M.D., Encinas-Lara, M.S., Escarzaga, S.M., Fernández-Guisuraga, J.M., Fisher, A.G., Gdulová, K., Gillespie, B.M., Griebel, A., Hanan, N.P., Hanggito, M.S., Haselberger, S., Havrilla, C.A., Heilman, P., Ji, W., Karl, J.W., Kirchhoff, M., Kraushaar, S., Lyons, M.B., Marzolff, I., Mauritz, M.E., McIntire, C.D., Metzen, D., Méndez-Barroso, L.A., Power, S.C., Prošek, J., Sanz-Ablanedo, E., Sauer, K.J., Schulze-Brüninghoff, D., Šímová, P., Sitch, S., Smit, J.L., Steele, C.M., Suárez-Seoane, S., Vargas, S.A., Villarreal, M., Visser, F., Wachendorf, M., Wirnsberger, H., Wojcikiewicz, R., 2022. Global application of an unoccupied aerial vehicle photogrammetry protocol for predicting aboveground biomass in non-forest ecosystems. Remote Sens. Ecol. Conserv. 8, 57–71. https://doi.org/10.1002/rse2.228.

Danby, R.K., 2011. Monitoring forest–tundra ecotones at multiple scales. Geogr. Compass 5, 623–640. https://doi.org/10.1111/j.1749-8198.2011.00447.x.

Dobbert, S., Pape, R., Löffler, J., 2021. How does spatial heterogeneity affect inter- and intraspecific growth patterns in tundra shrubs? J. Ecol. 109, 4115–4131. https://doi.org/10.1111/1365-2745.13784.

Erlandsson, R., Stoessel, M., Skånes, H., Wennbom, M., Angerbjörn, A., 2019. An innovative use of orthophotos – possibilities to assess plant productivity from colour infrared aerial orthophotos. Remote Sens. Ecol. Conserv. 5, 291–301. URL. https://onlinelibrary.wiley.com/doi/abs/10.1002/rse2.108. https://doi.org/10.1002/rse2.108._eprint. https://zslpublications.onlinelibrary.wiley.com/doi/pdf/10.1002/rse2.108.

Erlandsson, R., Bjerke, J.W., Finne, E.A., Myneni, R.B., Piao, S., Wang, X., Virtanen, T., Räsänen, A., Kumpula, T., Kolari, T.H.M., Tahvanainen, T., Tømmervik, H., 2022. An artificial intelligence approach to remotely assess pale lichen biomass. Remote Sens. Environ. 280, 113201 https://doi.org/10.1016/j.rse.2022.113201.

Fassnacht, F.E., Müllerová, J., Conti, L., Malavasi, M., Schmidtlein, S., 2022. About the link between biodiversity and spectral variation. Appl. Veg. Sci. 25, e12643. URL. https://onlinelibrary.wiley.com/doi/abs/10.1111/avsc.12643. https://doi.org/10.1111/avsc.12643._eprint. https://onlinelibrary.wiley.com/doi/pdf/10.1111/avsc.12643.

Feilhauer, H., Zlinszky, A., Kania, A., Foody, G.M., Doktor, D., Lausch, A., Schmidtlein, S., 2021. Let your maps be fuzzy!—class probabilities and floristic gradients as alternatives to crisp mapping for remote sensing of vegetation. Remote Sens. Ecol. Conserv. 7, 292–305. https://doi.org/10.1002/rse2.188.

Ferraro Brigida, M., Giordani, P., Serafini, A., 2019. Fclust: an R package for fuzzy clustering. The R J. 11, 198. https://doi.org/10.32614/RJ-2019-017.

Genuer, R., Poggi, J.M., Malot, C.T., 2015. VSURF: an R package for variable selection using random forests. The R J. 7, 19–33. https://doi.org/10.32614/RJ-2015-018.

Guisan, A., Weiss, S.B., Weiss, A.D., 1999. GLM versus CCA spatial modeling of plant species distribution. Plant Ecol. 143, 107–122. https://doi.org/10.1023/A:1009841519580.

Haapasaari, M., 1988. The Oligotrophic Heath Vegetation of Northern Fennoscandia and its Zonation. Doctoral Thesis. University of Helsinki, Helsinki. ISBN: 951–9469-29-X. Acta botanica Fennica: 135.

Hall, E.C., Lara, M.J., 2022. Multisensor UAS mapping of plant species and plant functional types in Midwestern grasslands. Remote Sens. 14, 3453. https://doi.org/10.3390/rs14143453.

Halme, E., Pellikka, P., Mõttus, M., 2019. Utility of hyperspectral compared to multispectral remote sensing data in estimating forest biomass and structure variables in Finnish boreal forest. Int. J. Appl. Earth Obs. Geoinf. 83, 101942. URL: https://www.sciencedirect.com/science/article/pii/S0303243419304179 https://doi.org/10.1016/j.jag.2019.101942.

Huete, A.R., 2012. Vegetation indices, remote sensing and forest monitoring. Geogr. Compass 6, 513–532. https://doi.org/10.1111/j.1749-8198.2012.00507.x.

Ju, J., Gopal, S., Kolaczyk, E.D., 2005. On the choice of spatial and categorical scale in remote sensing land cover classification. Remote Sens. Environ. 96, 62–77. URL. https://www.sciencedirect.com/science/article/pii/S0034425705000568. https://doi.org/10.1016/j.rse.2005.01.016.

Kim, D.M., Zhang, H., Zhou, H., Du, T., Wu, Q., Mockler, T.C., Berezin, M.Y., 2015. Highly sensitive image-derived indices of water-stressed plants using hyperspectral imaging in SWIR and histogram analysis. Sci. Rep. 5, 15919. URL. https://www.nature.com/articles/srep15919. https://doi.org/10.1038/srep15919. number: 1 Publisher: Nature Publishing Group.

Kou, D., Virtanen, T., Treat, C.C., Tuovinen, J.P., Räsänen, A., Juutinen, S., Mikola, J., Aurela, M., Heiskanen, L., Heikkilä, M., Weckström, J., Juselius, T., Piilo, S.R., Deng, J., Zhang, Y., Chaudhary, N., Huang, C., Väliranta, M., Biasi, C., Liu, X., Guo, M., Zhuang, Q., Korhola, A., Shurpali, N.J., 2022. Peatland heterogeneity impacts on regional carbon flux and its radiative effect within a boreal landscape. J. Geophys. Res. Biogeosci. 127 https://doi.org/10.1029/2021JG006774 e2021JG006774. URL.

Kupková, L., Červená, L., Potůčková, M., Lysák, J., Roubalová, M., Hrázský, Z., Březina, S., Epstein, H.E., Müllerová, J., 2023. Towards reliable monitoring of grass species in nature conservation: evaluation of the potential of UAV and PlanetScope multi-temporal data in the central European tundra. Remote Sens. Environ. 294, 113645. URL. https://www.sciencedirect.com/science/article/pii/S0034425723001967. https://doi.org/10.1016/j.rse.2023.113645.

Lang, M., Kuusk, A., Nilson, T., Lükk, T., Pehk, M., Alm, G.. Reflectance Spectra of Ground Vegetation in Sub-Boreal Forests. URL. https://www.aai.ee/bgf/ger2600/.

Lehnert, L.W., Meyer, H., Obermeier, W.A., Silva, B., Regeling, B., Thies, B., Bendix, J., 2019. Hyperspectral data analysis in R: the hsdar package. J. Stat. Softw. 89, 1–23. https://doi.org/10.18637/jss.v089.i12.

Liaw, A., Wiener, M., 2002. Classification and regression by randomForest. R News 2, 18–22. https://CRAN.R-project.org/doc/Rnews/.

Liu, N., Budkewitsch, P., Treitz, P., 2017. Examining spectral reflectance features related to Arctic percent vegetation cover: implications for hyperspectral remote sensing of Arctic tundra. Remote Sens. Environ. 192, 58–72. https://doi.org/10.1016/j.rse.2017.02.002.

Liu, S., Yan, Z., Wang, Z., Serbin, S., Visser, M., Zeng, Y., Ryu, Y., Su, Y., Guo, Z., Song, G., Wu, Q., Zhang, H., Cheng, K.H., Dong, J., Hau, B.C.H., Zhao, P., Yang, X., Liu, L., Rogers, A., Wu, J., 2023. Mapping foliar photosynthetic capacity in sub-tropical and tropical forests with UAS-based imaging spectroscopy: scaling from leaf to canopy. Remote Sens. Environ. 293, 113612. URL: https://www.sciencedirect.com/science/article/pii/S0034425723001633 https://doi.org/10.1016/j.rse.2023.113612.

Lu, B., He, Y., Dao, P.D., 2019. Comparing the performance of multispectral and hyperspectral images for estimating vegetation properties. IEEE J. Select. Top. Appl. Earth Observ. Remote Sens. 12, 1784–1797. URL. https://ieeexplore.ieee.org/abstract/document/8703822. https://doi.org/10.1109/JSTARS.2019.2910558. conference Name: IEEE Journal of Selected Topics in Applied Earth Observations and Remote Sensing.

Luo, G., Chen, G., Tian, L., Qin, K., Qian, S.E., 2016. Minimum noise fraction versus principal component analysis as a preprocessing step for hyperspectral imagery denoising. Can. J. Remote. Sens. 42, 106–116 publisher: Taylor & Francis _eprint. https://doi.org/10.1080/07038992.2016.1160772.

Madonsela, S., Cho, M.A., Ramoelo, A., Mutanga, O., 2017. Remote sensing of species diversity using Landsat 8 spectral variables. ISPRS J. Photogramm. Remote Sens. 133, 116–127. https://doi.org/10.1016/j.isprsjprs.2017.10.008.

McPartland, M.Y., Falkowski, M.J., Reinhardt, J.R., Kane, E.S., Kolka, R., Turetsky, M.R., Douglas, T.A., Anderson, J., Edwards, J.D., Palik, B., Montgomery, R.A., 2019. Characterizing boreal peatland plant composition and species diversity with hyperspectral remote sensing. Remote Sens. 11, 1685. https://doi.org/10.3390/rs11141685.

Mekonnen, Z.A., Riley, W.J., Berner, L.T., Bouskill, N.J., Torn, M.S., Iwahana, G., Breen, A.L., Myers-Smith, I.H., Criado, M.G., Liu, Y., Euskirchen, E.S., Goetz, S.J., Mack, M.C., Grant, R.F., 2021. Arctic tundra shrubification: a review of mechanisms and impacts on ecosystem carbon balance. Environ. Res. Lett. 16, 053001 https://doi.org/10.1088/1748-9326/abf28b.

MicaSense, 2020. MicaSense RedEdge-MX™ and DLS 2 Integration Guide. URL. https://support.micasense.com/hc/en-us/articles/360011389334-RedEdge-MX-Integration-Guide.

Minchin, P.R., 1987. An evaluation of the relative robustness of techniques for ecological ordination. In: Prentice, I.C., van der Maarel, E. (Eds.), Theory and Models in Vegetation Science: Proceedings of Symposium, Uppsala, July 8–13, 1985. Springer Netherlands, Dordrecht, pp. 89–107. https://doi.org/10.1007/978-94-009-4061-1_9.

Mod, H.K., Luoto, M., 2016. Arctic shrubification mediates the impacts of warming climate on changes to tundra vegetation. Environ. Res. Lett. 11, 124028. https://doi.org/10.1088/1748-9326/11/12/124028 publisher: IOP Publishing.

Myers-Smith, I.H., Kerby, J.T., Phoenix, G.K., Bjerke, J.W., Epstein, H.E., Assmann, J.J., John, C., Andreu-Hayles, L., Angers-Blondin, S., Beck, P.S.A., Berner, L.T., Bhatt, U.S., Bjorkman, A.D., Blok, D., Bryn, A., Christiansen, C.T., Cornelissen, J.H.C., Cunliffe, A.M., Elmendorf, S.C., Forbes, B.C., Goetz, S.J., Hollister, R.D., de Jong, R., Loranty, M.M., Macias-Fauria, M., Maseyk, K., Normand, S., Olofsson, J., Parker, T.C., Parmentier, F.J.W., Post, E., Schaepman-Strub, G., Stordal, F., Sullivan, P.F., Thomas, H.J.D., Tømmervik, H., Treharne, R., Tweedie, C.E., Walker, D.A., Wilmking, M., Wipf, S., 2020. Complexity revealed in the greening of the Arctic. Nat. Clim. Chang. 10, 106–117. https://doi.org/10.1038/s41558-019-0688-1.

Näsi, R., 2021. Drone-Based Spectral and 3D Remote Sensing Applications for Forestry and Agriculture. Doctoral Thesis.. Aalto University, Espoo, Finland.

National Land Survey of Finland. NLS orthophotos | National Land Survey of Finland. URL. https://www.maanmittauslaitos.fi/en/maps-and-spatial-data/datasets-and-interfaces/product-descriptions/orthophotos.

Nelson, P.R., Maguire, A.J., Pierrat, Z., Orcutt, E.L., Yang, D., Serbin, S., Frost, G.V., Macander, M.J., Magney, T.S., Thompson, D.R., Wang, J.A., Oberbauer, S.F., Zesati, S.V., Davidson, S.J., Epstein, H.E., Unger, S., Campbell, P.K.E., Carmon, N., Velez-Reyes, M., Huemmrich, K.F., 2022. Remote sensing of tundra ecosystems using high spectral resolution reflectance: opportunities and challenges. J. Geophys. Res. Biogeosci. 127 https://doi.org/10.1029/2021JG006697.

Nex, F., Armenakis, C., Cramer, M., Cucci, D.A., Gerke, M., Honkavaara, E., Kukko, A., Persello, C., Skaloud, J., 2022. UAV in the advent of the twenties: where we stand and what is next. ISPRS J. Photogramm. Remote Sens. 184, 215–242. URL: https://www.sciencedirect.com/science/article/pii/S0924271621003282 https://doi.org/10.1016/j.isprsjprs.2021.12.006.

Oksanen, L., Virtanen, R., 1995. Topographic, altitudinal and regional patterns in continentaland suboceanicheath vegetation of northern Fennoscandia. Acta Bot. Fenn. 153, 1–80.

Oksanen, J., Simpson, G.L., Blanchet, F.G., Kindt, R., Legendre, P., Minchin, P.R., O'Hara, R., Solymos, P., Stevens, M.H.H., Szoecs, E., Wagner, H., Barbour, M., Bedward, M., Bolker, B., Borcard, D., Carvalho, G., Chirico, M., De Caceres, M., Durand, S., Evangelista, H.B.A., FitzJohn, R., Friendly, M., Furneaux, B., Hannigan, G., Hill, M.O., Lahti, L., McGlinn, D., Ouellette, M.H., Ribeiro Cunha, E., Smith, T., Stier, A., Ter Braak, C.J., Weedon, J., 2022. vegan: Community Ecology Package. URL. https://CRAN.R-project.org/package=vegan.

Orndahl, K.M., Ehlers, L.P., Herriges, J.D., Pernick, R.E., Hebblewhite, M., Goetz, S.J., 2022. Mapping tundra ecosystem plant functional type cover, height, and aboveground biomass in Alaska and Northwest Canada using unmanned aerial vehicles. Arctic Sci. 8, 1165–1180. URL. https://cdnsciencepub.com/doi/full/10.1139/as-2021-0044. https://doi.org/10.1139/as-2021-0044. publisher: NRC Research Press.

Pääkkö, E., Mäkelä, K., Saikkonen, A., Tynys, S., Anttonen, M., Johansson, P., Kumpula, J., Mikkola, K., Norokorpi, Y., Suominen, O., et al., 2018. Tunturit. In: Suomen luontotyyppien uhanalaisuus 2018 : Luontotyyppien punainen kirja. Osa 2: Luontotyyppien kuvaukset. Suomen ympäristökeskus, Helsinki. number 5 in Suomen ympäristö, pp. 758–884.

Palmer, M.W., Earls, P.G., Hoagland, B.W., White, P.S., Wohlgemuth, T., 2002. Quantitative tools for perfecting species lists. Environmetrics 13, 121–137. URL: https://onlinelibrary.wiley.com/doi/abs/10.1002/env.516 https://doi.org/10.1002/env.516._eprint https://onlinelibrary.wiley.com/doi/pdf/10.1002/env.516.

Pang, Y., Räsänen, A., Lindholm, V., Aurela, M., Virtanen, T., 2022. Detecting peatland vegetation patterns with multi-temporal field spectroscopy. GISci. Remote Sens. 59, 2111–2126. https://doi.org/10.1080/15481603.2022.2152303.

Peanusaha, S., Pourreza, A., Kamiya, Y., Fidelibus, M.W., Chakraborty, M., 2024. Nitrogen retrieval in grapevine (*Vitis vinifera* L.) leaves by hyperspectral sensing. Remote Sens. Environ. 302, 113966. URL. https://www.sciencedirect.com/science/article/pii/S0034425723005187. https://doi.org/10.1016/j.rse.2023.113966.

Poley, L.G., McDermid, G.J., 2020. A systematic review of the factors influencing the estimation of vegetation aboveground biomass using unmanned aerial systems. Remote Sens. 12, 1052. https://doi.org/10.3390/rs12071052.

R Core Team, 2021. R: A Language and Environment for Statistical Computing. R Foundation for Statistical Computing, Vienna, Austria. https://www.R-project.org/.

Rantanen, M., Karpechko, A.Y., Lipponen, A., Nordling, K., Hyvärinen, O., Ruosteenoja, K., Vihma, T., Laaksonen, A., 2022. The Arctic has warmed nearly four times faster than the globe since 1979. Commun. Earth Environ. 3, 1–10. https://doi.org/10.1038/s43247-022-00498-3.

Rapinel, S., Rossignol, N., Hubert-Moy, L., Bouzillé, J.B., Bonis, A., 2018. Mapping grassland plant communities using a fuzzy approach to address floristic and spectral uncertainty. Appl. Veg. Sci. 21, 678–693. https://doi.org/10.1111/avsc.12396.

Räsänen, A., Virtanen, T., 2019. Data and resolution requirements in mapping vegetation in spatially heterogeneous landscapes. Remote Sens. Environ. 230, 111207 https://doi.org/10.1016/j.rse.2019.05.026.

Räsänen, A., Juutinen, S., Aurela, M., Virtanen, T., 2019a. Predicting aboveground biomass in Arctic landscapes using very high spatial resolution satellite imagery and field sampling. Int. J. Remote Sens. 40, 1175–1199. https://doi.org/10.1080/01431161.2018.1524176.

Räsänen, A., Juutinen, S., Tuittila, E.S., Aurela, M., Virtanen, T., 2019b. Comparing ultra-high spatial resolution remote-sensing methods in mapping peatland vegetation. J. Veg. Sci. 30, 1016–1026. https://doi.org/10.1111/jvs.12769.

Räsänen, A., Aurela, M., Juutinen, S., Kumpula, T., Lohila, A., Penttilä, T., Virtanen, T., 2020a. Detecting northern peatland vegetation patterns at ultra-high spatial resolution. Remote Sens. Ecol. Conserv. 6, 457–471. https://doi.org/10.1002/rse2.140.

Räsänen, A., Juutinen, S., Kalacska, M., Aurela, M., Heikkinen, P., Mäenpää, K., Rimali, A., Virtanen, T., 2020b. Peatland leaf-area index and biomass estimation with ultra-high resolution remote sensing. GISci. Remote Sens. 57, 943–964. https://doi.org/10.1080/15481603.2020.1829377.

Räsänen, A., Manninen, T., Korkiakoski, M., Lohila, A., Virtanen, T., 2021a. Predicting catchment-scale methane fluxes with multi-source remote sensing. Landsc. Ecol. 36, 1177–1195. https://doi.org/10.1007/s10980-021-01194-x.

Räsänen, A., Wagner, J., Hugelius, G., Virtanen, T., 2021b. Aboveground biomass patterns across treeless northern landscapes. Int. J. Remote Sens. 42, 4536–4561. https://doi.org/10.1080/01431161.2021.1897187.

Rehman, T.U., Ma, D., Wang, L., Zhang, L., Jin, J., 2020. Predictive spectral analysis using an end-to-end deep model from hyperspectral images for high-throughput plant phenotyping. Comput. Electron. Agric. 177, 105713. URL: https://www.sciencedirect.com/science/article/pii/S0168169920315908 https://doi.org/10.1016/j.compag.2020.105713.

Reichle, L.M., Epstein, H.E., Bhatt, U.S., Raynolds, M.K., Walker, D.A., 2018. Spatial heterogeneity of the temporal dynamics of Arctic tundra vegetation. Geophys. Res. Lett. 45, 9206–9215. https://doi.org/10.1029/2018GL078820.

Rocchini, D., Balkenhol, N., Carter, G.A., Foody, G.M., Gillespie, T.W., He, K.S., Kark, S., Levin, N., Lucas, K., Luoto, M., Nagendra, H., Oldeland, J., Ricotta, C., Southworth, J., Neteler, M., 2010. Remotely sensed spectral heterogeneity as a proxy of species diversity: recent advances and open challenges. Eco. Inform. 5, 318–329. URL: https://www.sciencedirect.com/science/article/pii/S1574954110000646 https://doi.org/10.1016/j.ecoinf.2010.06.001.

Shannon, C.E., 1948. A mathematical theory of communication. Bell Syst. Tech. J. 27, 379–423. https://doi.org/10.1002/j.1538-7305.1948.tb01338.x.

Steenvoorden, J., Bartholomeus, H., Limpens, J., 2023. Less is more: optimizing vegetation mapping in peatlands using unmanned aerial vehicles (UAVs). Int. J. Appl. Earth Obs. Geoinf. 117, 103220. URL: https://www.sciencedirect.com/science/article/pii/S1569843223000420 https://doi.org/10.1016/j.jag.2023.103220.

Sundqvist, M.K., Sanders, N.J., Dorrepaal, E., Lindén, E., Metcalfe, D.B., Newman, G.S., Olofsson, J., Wardle, D.A., Classen, A.T., 2020. Responses of tundra plant community carbon flux to experimental warming, dominant species removal and elevation. Funct. Ecol. 34, 1497–1506. https://doi.org/10.1111/1365-2435.13567.

Thomson, E.R., Spiegel, M.P., Althuizen, I.H.J., Bass, P., Chen, S., Chmurzynski, A., Halbritter, A.H., Henn, J.J., Jónsdóttir, I.S., Klanderud, K., Li, Y., Maitner, B.S., Michaletz, S.T., Niittynen, P., Roos, R.E., Telford, R.J., Enquist, B.J., Vandvik, V., Macias-Fauria, M., Malhi, Y., 2021. Multiscale mapping of plant functional groups and plant traits in the high Arctic using field spectroscopy, UAV imagery and sentinel-2A data. Environ. Res. Lett. 16, 055006. https://doi.org/10.1088/1748-9326/abf464 publisher: IOP Publishing.

Treharne, R., Bjerke, J.W., Tømmervik, H., Stendardi, L., Phoenix, G.K., 2019. Arctic browning: impacts of extreme climatic events on heathland ecosystem CO2 fluxes. Glob. Chang. Biol. 25, 489–503. URL. https://onlinelibrary.wiley.com/doi/abs/10.1111/gcb.14500. https://doi.org/10.1111/gcb.14500._eprint. https://onlinelibrary.wiley.com/doi/pdf/10.1111/gcb.14500.

Tuovinen, J.P., Aurela, M., Hatakka, J., Räsänen, A., Virtanen, T., Mikola, J., Ivakhov, V., Kondratyev, V., Laurila, T., 2019. Interpreting eddy covariance data from heterogeneous Siberian tundra: land-cover-specific methane fluxes and spatial representativeness. Biogeosciences 16, 255–274. https://doi.org/10.5194/bg-16-255-2019.

Turner, D.P., Ollinger, S.V., Kimball, J.S., 2004. Integrating remote sensing and ecosystem process models for landscape- to regional-scale analysis of the carbon cycle. BioScience 54, 573–584. URL. https://doi.org/10.1641/0006-3568(2004)054[0573:IRSAEP]2.0.CO;2.

Turner, D.J., Malenovský, Z., Lucieer, A., Turnbull, J.D., Robinson, S.A., 2019. Optimizing spectral and spatial resolutions of unmanned aerial system imaging sensors for monitoring Antarctic vegetation. IEEE J. Select. Top. Appl. Earth Observ. Remote Sens. 12, 3813–3825. https://doi.org/10.1109/JSTARS.2019.2938544.

van der Merwe, S., Greve, M., Skowno, A.L., Hoffman, M.T., Cramer, M.D., 2023. Can vegetation be discretely classified in species-poor environments? Testing plant community concepts for vegetation monitoring on sub-Antarctic Marion Island. Ecol. Evol. 13, e9681. URL. https://onlinelibrary.wiley.com/doi/abs/10.1002/ece3.9681. https://doi.org/10.1002/ece3.9681._eprint. https://onlinelibrary.wiley.com/doi/pdf/10.1002/ece3.9681.

Villoslada, M., Ylänne, H., Juutinen, S., Kolari, T.H.M., Korpelainen, P., Tahvanainen, T., Wolff, F., Kumpula, T., 2023. Reindeer control over shrubification in subarctic wetlands: spatial analysis based on unoccupied aerial vehicle imagery. Remote Sens. Ecol. Conserv. 9, 687–706. URL. https://onlinelibrary.wiley.com/doi/abs/10.1002/rse2.337. https://doi.org/10.1002/rse2.337._eprint. https://onlinelibrary.wiley.com/doi/pdf/10.1002/rse2.337.

Virtanen, T., Ek, M., 2014. The fragmented nature of tundra landscape. Int. J. Appl. Earth Obs. Geoinf. 27, 4–12. https://doi.org/10.1016/j.jag.2013.05.010.

Wang, R., Gamon, J.A., 2019. Remote sensing of terrestrial plant biodiversity. Remote Sens. Environ. 231, 111218. URL. https://www.sciencedirect.com/science/article/pii/S0034425719302317. https://doi.org/10.1016/j.rse.2019.111218.

Yang, D., Meng, R., Morrison, B.D., McMahon, A., Hantson, W., Hayes, D.J., Breen, A.L., Salmon, V.G., Serbin, S.P., 2020. A multi-sensor unoccupied aerial system improves characterization of vegetation composition and canopy properties in the Arctic tundra. Remote Sens. 12, 2638. https://www.mdpi.com/2072-4292/12/16/2638. https://doi.org/10.3390/rs12162638. number: 16 Publisher: Multidisciplinary Digital Publishing Institute.

Yang, D., Morrison, B.D., Hantson, W., Breen, A.L., McMahon, A., Li, Q., Salmon, V.G., Hayes, D.J., Serbin, S.P., 2021. Landscape-scale characterization of Arctic tundra vegetation composition, structure, and function with a multi-sensor unoccupied aerial system. Environ. Res. Lett. 16, 085005. https://doi.org/10.1088/1748-9326/ac1291 publisher: IOP Publishing.